bioRxiv preprint doi: https://doi.org/10.1101/2020.01.22.916221; this version posted January 30, 2020. The copyright holder for this preprint (which was not certified by peer review) is the author/funder, who has granted bioRxiv a license to display the preprint in perpetuity. It is made available under aCC-BY-ND 4.0 International license.

Prolonged disturbance of proteostasis induces cellular senescence via temporal mitochondrial dysfunction and enhanced mitochondrial biogenesis in human fibroblasts

Authors: Yasuhiro Takenaka[1,2], Ikuo Inoue[2], Takanari Nakano[3], Masaaki Ikeda[4], Yoshihiko Kakinuma[1]

Affiliations: [1]Department of Physiology, Graduate School of Medicine, Nippon Medical School, Tokyo, Japan

[2]Department of Diabetes and Endocrinology, Saitama Medical University, Saitama, Japan

[3]Department of Biochemistry, Saitama Medical University, Saitama, Japan

[4]Department of Physiology, Saitama Medical University, Saitama, Japan

Correspondence

Yasuhiro Takenaka, PhD, Department of Physiology, Graduate School of Medicine, Nippon Medical School, Sendagi, Bunkyo-ku, Tokyo 113-8602, Japan, E-mail: yasuhiro-takenaka@nms.ac.jp

Key words: aging, mitochondria, oxidative stress, proteasome, lysosome, DNA damage response

bioRxiv preprint doi: https://doi.org/10.1101/2020.01.22.916221; this version posted January 30, 2020. The copyright holder for this preprint (which was not certified by peer review) is the author/funder, who has granted bioRxiv a license to display the preprint in perpetuity. It is made available under aCC-BY-ND 4.0 International license.

Abstract

Proteolytic activities decline with age, resulting in the accumulation of aggregated proteins in aged organisms. To investigate how disturbance of proteostasis causes cellular senescence in proliferating cells, we developed a stress-induced premature senescence (SIPS) model, in which normal human fibroblast MRC-5 cells were treated with either the proteasome inhibitor MG132 or V-ATPase inhibitor bafilomycin A1 (BAFA1). After 5 days of drug treatment, cells showed morphological and functional changes associated with aging along with DNA damage response. Time-course studies revealed significant increase in intracellular and mitochondrial reactive oxygen species (ROS) during and after drug treatment. We also found temporal downregulation of mitochondrial membrane potential during drug treatment, followed by an increase in mitochondrial mass, especially after drug treatment. Notable upregulation of PGC-1α and TFAM proteins confirmed enhanced mitochondrial biogenesis. Furthermore, the protein levels of SOD2 and GPx4, mitochondrial antioxidant enzymes, in the mitochondrial fraction were specifically reduced on day 1 of the treatment. Co-treatment with rapamycin along with MG132 or BAFA1 partially attenuated induction of SIPS by suppressing generation of excess ROS and mitochondrial biogenesis. In conclusion, the present study

bioRxiv preprint doi: https://doi.org/10.1101/2020.01.22.916221; this version posted January 30, 2020. The copyright holder for this preprint (which was not certified by peer review) is the author/funder, who has granted bioRxiv a license to display the preprint in perpetuity. It is made available under aCC-BY-ND 4.0 International license.

revealed that disturbance of proteostasis by the inhibitors changes the distribution of nuclear-encoded mitochondrial antioxidant enzymes at an early period of the treatment, which induces mitochondrial ROS and temporal mitochondrial dysfunction. ROS in turn activates stress responses pathways, followed by PGC-1α-mediated mitochondrial biogenesis. Hence, the excessive ROS continuously generated by increased mitochondria can cause deleterious damage to nuclear DNA, cell cycle arrest, and eventual cellular senescence.

bioRxiv preprint doi: https://doi.org/10.1101/2020.01.22.916221; this version posted January 30, 2020. The copyright holder for this preprint (which was not certified by peer review) is the author/funder, who has granted bioRxiv a license to display the preprint in perpetuity. It is made available under aCC-BY-ND 4.0 International license.

Introduction

Proteolytic activities and the rate of protein turnover decline in aged animals [1, 2] and humans [3]. The decline of proteostasis causes intracellular accumulation of crosslinked protein aggregates [4] and/or autofluorescent materials called lipofuscin [5] that are prominent markers for cellular senescence. Cellular senescence is characterized by permanent cell cycle arrest, morphological changes such as flattened cellular shape, increased levels of lysosome, upregulation of cyclin-dependent kinase (CDK) inhibitors p16 and p21 [6], enhanced activity of mTOR pathway [7], occurrence of medium levels of p53 [8], and expression of senescence associated β-galactosidase (SA-β-gal) [9]. Normal human fibroblasts, cultured *in vitro*, have limited proliferative capacity, which is known as the "Hayflick limit". Limited replicative potential and occurrence of replicative senescence are considered to be caused by a shortened telomere that triggers a DNA damage response (DDR) and eventual irreversible cell cycle arrest. On the other hand, stress-induced premature senescence (SIPS) can be induced via several stressors in young proliferative cells that have long and functional telomeres. Several factors have been reported to serve as inducers of SIPS, including DNA damaging reagents [10], producers of reactive oxygen species (ROS), expression of oncogenic genes [11], and several proteasome inhibitors.

bioRxiv preprint doi: https://doi.org/10.1101/2020.01.22.916221; this version posted January 30, 2020. The copyright holder for this preprint (which was not certified by peer review) is the author/funder, who has granted bioRxiv a license to display the preprint in perpetuity. It is made available under aCC-BY-ND 4.0 International license.

MG132, a tripeptide aldehyde, is a reversible inhibitor of β1 caspase-like, β2 trypsin-like, and β5 chymotrypsin-like activities of 20S proteasome. At a high dose, MG132 increases ROS levels and GSH depletion in human pulmonary fibroblasts [12], Chinese hamster ovary cells [13], and human leukemic cells [14], which results in cell death. When human fibroblasts, including MRC-5 cells, are treated with a low dose of MG132 for a long period, irreversible growth arrest and premature senescence can be observed [15-17]. This indicates that prolonged disturbance of proteostasis could cause premature senescence by a stress. However, the exact mechanisms underlying SIPS caused by proteasome inhibitors are unknown.

Mitochondria are the central organelles responsible for ATP generation as a source of energy supply in eukaryotic cells. During oxidative phosphorylation (OXPHOS) in mitochondria, electron transfer via an electron transport chain in complexes I and III can cause leakage of electrons [18], which is considered to be the major source of intracellular superoxide, hydrogen peroxide, and other downstream ROS such as hydroxyl radicals. The role of mitochondria in aging is more complicated. According to the mitochondrial free radical theory of aging, cumulative damages to mitochondrial DNA and proteins by ROS generated via OXPHOS hamper mitochondrial function and result in more ROS production [19]. This is a vicious cycle in which ROS causes successive

bioRxiv preprint doi: https://doi.org/10.1101/2020.01.22.916221; this version posted January 30, 2020. The copyright holder for this preprint (which was not certified by peer review) is the author/funder, who has granted bioRxiv a license to display the preprint in perpetuity. It is made available under aCC-BY-ND 4.0 International license.

mitochondrial damage, and mitochondrial dysfunction in turn produces more ROS, eventually leading to cellular senescence. Thus, accumulation of dysfunctional mitochondria seems to be one of the hallmarks in senescent cells. Moreover, increase in mitochondrial mass occurs in fibroblasts that undergo replicative senescence [20], SIPS [20, 21], and oncogene-induced senescence [11]. In many cases, accumulated mitochondria in senescent cells also show decreased mitochondrial membrane potential, which indicates mitochondrial dysfunction and increased ROS production, although the levels of mitochondrial superoxide and hydrogen peroxide increase or decrease is dependent on the cause of the dysfunction [18].

In this study, we investigated the mechanisms underlying the induction of premature senescence in young human fibroblast MRC-5 cells that show Hayflick limit at around 60 population doubling level (PDL), by prolonged treatment with MG132 or bafilomycin A1 (BAFA1). BAFA1, a plecomacrolide, is a specific and potent inhibitor of vacuolar-type ATPases (V-ATPases), a proton pump that acidifies lysosomes, which subsequently inhibit lysosomal degradation of biomolecules from several clearance pathways, including macroautophagy and mitophagy [22]. In the current study, both MG132 and BAFA1 impaired cellular proteostasis and induced premature senescence in MRC-5 cells in a similar manner, although the target molecules of the two drugs are different. To

bioRxiv preprint doi: https://doi.org/10.1101/2020.01.22.916221; this version posted January 30, 2020. The copyright holder for this preprint (which was not certified by peer review) is the author/funder, who has granted bioRxiv a license to display the preprint in perpetuity. It is made available under aCC-BY-ND 4.0 International license.

elucidate the exact mechanisms of SIPS by these drugs, we performed time-course studies on senescence-associated markers, ROS, DDR, and mitochondrial function and biogenesis during and after treatment with MG132 and BAFA1. We demonstrated that the initial loss of mitochondrial functions is possibly caused by temporal depletion of mitochondrial antioxidant proteins and sequential increase in mitochondrial ROS, which in turn could induce mitochondrial biogenesis, excess production of intracellular ROS, DDR, and eventual cellular senescence.

Results

Prolonged disturbance of proteostasis by MG132 or BAFA1 induces cell cycle arrest, DNA damage response, and SIPS in early passage human fibroblasts

To elucidate how prolonged inhibition of proteostasis induces premature senescence in fibroblasts, we first established a MG132- or BAFA1-induced cellular senescence model. We exposed normal human fibroblast MRC-5 cells (36-39 PDL) to low concentration of MG132 (0.1 μM) or BAFA1 (4 nM) for 3 or 5 days (Fig. 1A). During MG132 or BAFA1 treatment for 5 consecutive days, the cells almost stopped proliferation and acquired thin needle-like morphology (Fig. S1A, day 3). When the culture medium was returned to the regular medium without the inhibitor (Fig. 1A), sustained

bioRxiv preprint doi: https://doi.org/10.1101/2020.01.22.916221; this version posted January 30, 2020. The copyright holder for this preprint (which was not certified by peer review) is the author/funder, who has granted bioRxiv a license to display the preprint in perpetuity. It is made available under aCC-BY-ND 4.0 International license.

growth arrest was observed (Fig. 1B). After drug removal, the cells gradually changed in morphology, that is, to enlarged flat shape at around 3-4 post-treatment days (PD)(Fig. S1A, PD5), which generally occurs during senescence. However, when cells were treated with the same concentration of MG132 or BAFA1 for 3 consecutive days, proliferation was resumed after drug removal (Fig. 1B). Induction of SIPS was also evaluated by conventional SA-β-gal staining and cell-based microplate assay using SPiDER-βGal, a fluorogenic substrate for β-galactosidase. In cells treated with either of the drugs for 5 consecutive days, SA-β-gal-positive cells were clearly observed at PD7; whereas no such cells were observed when treated for 3 days (Fig. 1C). Therefore, we performed a 5-day treatment with either of the drugs for all the experiments discussed further in this report. Cell-based assay for SA-β-gal activity confirmed significant increase in the activity in cells at PD3 and PD6 after treatment with MG132 (Fig. 1D, left) and BAFA1 (Fig. 1D, right) for 5 days. We also observed remarkable increase in aggresome-like inclusion bodies that were morphologically similar to those in cells undergoing replicative senescence (58 PDL) as early as day 1 of treatment with MG132 or BAFA1 (Fig. 1E). The aggregates were detectable even at PD6.

Further, we investigated the induction of DDR by monitoring the expression of activated H2AX (γH2A.X) during and after treatment of MG132 or BAFA1. DNA damage foci were

bioRxiv preprint doi: https://doi.org/10.1101/2020.01.22.916221; this version posted January 30, 2020. The copyright holder for this preprint (which was not certified by peer review) is the author/funder, who has granted bioRxiv a license to display the preprint in perpetuity. It is made available under aCC-BY-ND 4.0 International license.

observed in nuclei of cells at PD5 (Fig. 1F). In immunoblot analyses, protein levels of γH2A.X were relatively repressed during treatment but increased after the drug removal in both drug-treated cells (Fig. 1G). We also performed time-course analyses of senescence-associated marker proteins. CDK inhibitor p21 levels were increased as early as day 1 and remained predominantly the same thereafter, indicating prompt and sustained cell cycle arrest (Fig. 1G). Prolonged and low-level expression of p53, which is one of the hallmarks of cellular senescence [8], was also detected during and after drug treatments. The p21 and p53 levels were comparable to control MRC-5 cells that underwent replicative senescence (Fig. S1B, 55 and 60 PDL). Sustained activation of mTOR has been reported to be required for cellular senescence [23, 24]. Phosphorylated ribosomal protein S6 (p-S6), a target of mTORC1, depleted once during drug treatment, but recovered to the initial level (control) after the treatment (Fig. 1G), indicating restoration of the growth signal in cells that ceased to proliferate (Fig. 1B). Both NRF1 and NRF2, NF-E2-related factor 1 and 2 respectively, were transiently upregulated at a very early period of MG132 treatment (Fig. 1H), but depleted thereafter (Fig. S2A). In BAFA1-treated cells, very weak induction of NRF1 and NRF2 at 48 hrs was observed (Fig. 1I). We also investigated metabolic remodeling as seen in some senescent cells, which showed upregulation of both OXPHOS and glycolysis [25]. The protein levels of glucose transporter GLUT1

bioRxiv preprint doi: https://doi.org/10.1101/2020.01.22.916221; this version posted January 30, 2020. The copyright holder for this preprint (which was not certified by peer review) is the author/funder, who has granted bioRxiv a license to display the preprint in perpetuity. It is made available under aCC-BY-ND 4.0 International license.

137 and HIF-1α that induces several glycolytic proteins did not increase in MG132- and BAFA1-treated

138 cells (Fig. S2B), implying that there was no shift toward glycolysis in our SIPS model.

139 We have also tested for SIPS induction in rat H9c2 myoblasts by MG132 or BAFA1 with

140 the same treatment regimen as adopted in MRC-5 cells, which demonstrated that SIPS induction by

141 these inhibitors is not a specific feature of human fibroblasts (data not shown).

142

143 **Prolonged treatment of MG132 or BAFA1 increases intracellular ROS, H_2O_2, and**

144 **mitochondrial ROS, but not NO**

145 Treatment of cells with various doses (1-30 μM) of MG132 increases intracellular ROS [12, 26] and

146 NO production [14], but the kinetics of ROS/NO production in fibroblasts during and after longer

147 treatment with MG132 or BAFA1 is unknown. During MG132 or BAFA1 treatment, intracellular

148 H_2O_2 and hydroxyl radical ($^{\cdot}$OH) levels detected by HYDROP and OxiORANGE, respectively, did

149 not increase on day 1 but gradually increased from day 3. From PD1 to PD5, hydroxyl radical (Fig.

150 2A and 2B) and H_2O_2 (Fig. 2C and 2D) levels were still higher than that of control cells.

151 Contrastingly, NO levels detected by DAF-FM DA fluorescent dye remained largely unchanged or

152 slightly reduced during and after treatments with either drug (Fig. S3). There was no increase in

bioRxiv preprint doi: https://doi.org/10.1101/2020.01.22.916221; this version posted January 30, 2020. The copyright holder for this preprint (which was not certified by peer review) is the author/funder, who has granted bioRxiv a license to display the preprint in perpetuity. It is made available under aCC-BY-ND 4.0 International license.

153 mRNA and protein levels of inducible NOS (data not shown), which confirmed that NO was not the

154 cause of senescence induction in MG132- and BAFA1-treated cells.

155 To reveal the involvement of mitochondria in an increased production of intracellular

156 ROS in MG132- or BAFA1-treated cells, we assessed mitochondrial ROS levels using MitoSOX

157 superoxide indicator. Mitochondrial ROS levels significantly increased in both MG132- and

158 BAFA1-treated cells as early as day 1 of the treatment and peaked at PD3 (Fig. 2E and 2F).

159

160 **Prolonged treatment of MG132 or BAFA1 enhances mitochondrial biogenesis**

161 We next investigated changes in mitochondrial mass and mitochondrial membrane potential (Δψm)

162 using MitoTracker Green FM and MitoTracker Red CM-H2Xros, respectively. In either drug-treated

163 cells, mitochondrial mass gradually increased during treatment and remained at high levels even

164 after treatment (Fig. 3A and 3C, mitochondrial mass (Mt mass)). Contrarily, the mitochondrial

165 membrane potential increased once on day 1, compared with untreated control cells, but slightly

166 decreased on days 3 and 5, and markedly increased thereafter (Fig. 3B and 3C, Δψm).

167 Mitochondrial proliferation was also confirmed by qPCR analyses of mitochondrial DNA (mtDNA)

168 copy number (Fig. 3D). Intracellular ATP were almost at basal levels during treatment, but increased

bioRxiv preprint doi: https://doi.org/10.1101/2020.01.22.916221; this version posted January 30, 2020. The copyright holder for this preprint (which was not certified by peer review) is the author/funder, who has granted bioRxiv a license to display the preprint in perpetuity. It is made available under aCC-BY-ND 4.0 International license.

169 thereafter (Fig. 3E), which may reflect the restoration of mitochondrial membrane potential after
170 drug treatment. These results suggest temporal mitochondrial dysfunction during drug treatment but
171 accumulation of functional mitochondria, probably by mitochondrial biogenesis, thereafter.

172 We further explored how mitochondrial mass increased in MG132- or BAFA1-treated
173 cells by assessing protein expression of key factors in mitochondrial biogenesis and clearance.
174 PGC-1α, the master regulator of mitochondrial biogenesis, was upregulated temporarily from day 3
175 to PD1 with different kinetics between MG132 and BAFA1, but downregulated thereafter (Fig. 3F).
176 In contrast, TFAM, the key mitochondrial transcription activator, was consistently elevated during
177 and after treatment. Upregulation of these factors indicated enhanced mitochondrial biogenesis in
178 MG132- and BAFA1-treated cells. Furthermore, Parkin, the ubiquitin ligase that is responsible for
179 mitophagy, was largely downregulated below basal levels, indicating suppression of mitophagic flux
180 during and after treatment. We also found that AMP-activated protein kinase alpha (AMPKα) was
181 remarkably activated, especially on days 3 and 5 (Fig. 3F), which is consistent with increase in
182 intracellular ATP levels in post-treatment periods (Fig. 3E). Increase in cytochrome c oxidase
183 subunit 4 (COX4) levels also confirmed an increase in mitochondrial mass in MG132- and
184 BAFA1-treated cells.

bioRxiv preprint doi: https://doi.org/10.1101/2020.01.22.916221; this version posted January 30, 2020. The copyright holder for this preprint (which was not certified by peer review) is the author/funder, who has granted bioRxiv a license to display the preprint in perpetuity. It is made available under aCC-BY-ND 4.0 International license.

MG132- or BAFA1-treatment causes reduction in mitochondrial antioxidant proteins in mitochondrial fraction during the early period of treatment

Recently, mass spectrometry analysis revealed aggregation of nuclear-encoded mitochondrial proteins such as respiratory chain complex subunits as an early event in MG132-treated cells [27]. In our experiments, mitochondrial ROS was significantly increased in MG132- or BAFA1-treated cells as early as day 1 compared with untreated control cells (Fig. 2E), implying that enhanced ROS generation and/or failure to scavenge ROS occur in the mitochondria immediately after initiation of drug treatment. Thus, we investigated protein levels of two mitochondrial antioxidant enzymes, superoxide dismutase (SOD2) and glutathione peroxidase (GPx4), in biochemically isolated mitochondrial fraction (detailed method in Fig. S4A) of MG132- or BAFA1-treated cells. On day 1, SOD2 was depleted specifically in mitochondrial fraction (Fig. 4A, Mt) in either drug-treated cells although the overall SOD2 level was almost constant or slightly increased compared with control cells (Fig. 4A, whole). From day 3, whole and mitochondrial SOD2 levels notably increased. Similarly, GPx4 in mitochondrial fraction was also depleted on day 1 and induced thereafter. We also observed reduction in NDUFS3, NADH dehydrogenase ubiquinone iron-sulfur protein 3 of

bioRxiv preprint doi: https://doi.org/10.1101/2020.01.22.916221; this version posted January 30, 2020. The copyright holder for this preprint (which was not certified by peer review) is the author/funder, who has granted bioRxiv a license to display the preprint in perpetuity. It is made available under aCC-BY-ND 4.0 International license.

respiratory complex 1, in mitochondrial fraction on day 1, which was in accordance with results from mass spectrometry analysis and observation of Ndufs3-EGFP localization in MG132-treated cells, reported in a previous study [27]. In contrast, the protein levels of Tom40 and GAPDH in mitochondrial fraction remained largely unchanged in either drug-treated cells. We also observed accumulation of aggregate-like particles of SOD2 in the cytoplasm of either MG132- or BAFA1-treated cells on day 1 (Fig. 4B). These results suggest that antioxidant enzymes could form aggregates before translocation into mitochondria, as an early event of disturbance of proteostasis, which eventually reduces mitochondrial ROS-scavenging efficiency.

Rapamycin treatment partially attenuates cellular senescence induced by MG132 or BAFA1

Mitochondrial function and biogenesis are controlled by mTOR [28]. Inhibition of mTOR by rapamycin, a mTORC1 inhibitor, resulted in a decrease in mitochondrial oxidative function [29], mitochondrial ROS [30], and senescence induction [31-33]. To further investigate the involvement of mitochondrial biogenesis in our SIPS model, we co-treated cells with rapamycin and either MG132 or BAFA1. In the case of 5 days co-treatment with rapamycin and MG132 or BAFA1 from day 0 (Fig. 5A, Rapa1), cells recovered proliferation potential after PD5 (Fig. 5B). In contrast, poor

bioRxiv preprint doi: https://doi.org/10.1101/2020.01.22.916221; this version posted January 30, 2020. The copyright holder for this preprint (which was not certified by peer review) is the author/funder, who has granted bioRxiv a license to display the preprint in perpetuity. It is made available under aCC-BY-ND 4.0 International license.

217 growth was observed in cells co-treated for 2 days from day 3 and additionally treated with only
218 rapamycin for 3 days from PD1 (Fig. 5A and 5B, Rapa2). The effects of rapamycin on SIPS were
219 also confirmed by SA-β-gal activity (Fig. 5C and S5) and intracellular H_2O_2 levels (Fig. 5D and 5E)
220 in both MG132- and BAFA1-treated cells. Furthermore, an increase in mitochondrial mass, assessed
221 by MitoTracker Green, was significantly repressed by co-treatment with rapamycin and either
222 MG132 (Rapa1) or BAFA1 (Rapa1 and Rapa2) (Fig. 5F). Different profiles of proliferative potential,
223 H_2O_2 levels, and mitochondrial mass between Rapa1 and Rapa2 suggested that cellular events during
224 the early period (days 0-3) of drug treatment intensively affect the following SIPS progression. Thus,
225 we further analyzed rapamycin effect on ROS production during early period (days 1-2) of the
226 treatment. Mitochondrial ROS significantly decreased by co-treatment with rapamycin on day 1
227 (MG132) or day 2 (BAFA1) compared with cells only treated with either MG132 or BAFA1 (Fig.
228 5G). Furthermore, protein contents of SOD2 in both whole and mitochondrial fractions increased in
229 cells co-treated with rapamycin and BAFA1, whereas those of GPx4 increased in cells co-treated
230 with rapamycin and MG132 (Fig. 5H), showing an accelerated upregulation and proper translocation
231 of mitochondrial anti-oxidant enzymes by rapamycin co-treatment.

232 Further, we evaluated significance of ROS produced during the early period of treatment

bioRxiv preprint doi: https://doi.org/10.1101/2020.01.22.916221; this version posted January 30, 2020. The copyright holder for this preprint (which was not certified by peer review) is the author/funder, who has granted bioRxiv a license to display the preprint in perpetuity. It is made available under aCC-BY-ND 4.0 International license.

in mitochondrial biogenesis. Cells were co-treated with *N*-acetyl-L-cysteine (NAC), a ROS scavenger, and either MG132 or BAFA1 for 2 days with 3 different starting dates (Fig. 6A, NAC1-3). In both MG132- and BAFA1-treated cells, co-treatment of NAC during the initial 2 days (NAC1) showed the highest suppression in the increase in mitochondrial mass at PD2 (Fig. 6B), implying that ROS produced during the early period (days 1-2) greatly triggered mitochondrial biogenesis.

Discussion

Previous studies have shown that SIPS is induced in human fibroblasts by treatment of proteasome inhibitors such as MG132 [15-17]. However, the exact mechanisms of SIPS induction by proteasome inhibition have not been clarified. In this study, we found that the prolonged disturbance of proteostasis by not only MG132 but also by BAFA1, an inhibitor of lysosome function, induces SIPS through early temporal mitochondrial dysfunction, sequential mitochondrial biogenesis that possibly enhances excess ROS production, and eventual DDR. Notably, SIPS by MG132 and BAFA1 showed similar phenotypes and kinetics of senescence-associated markers, mitochondrial dysfunction and biogenesis, ROS levels, and DDR, although these reagents inhibit different

bioRxiv preprint doi: https://doi.org/10.1101/2020.01.22.916221; this version posted January 30, 2020. The copyright holder for this preprint (which was not certified by peer review) is the author/funder, who has granted bioRxiv a license to display the preprint in perpetuity. It is made available under aCC-BY-ND 4.0 International license.

249 molecules, chymotrypsin-like protease in 20S proteasome and proton pump V-ATPase on lysosome
250 membrane, respectively. This implies the presence of shared mechanisms in SIPS induced by
251 disturbance of proteostasis regardless of initial causes. Contrastingly, there are several differences
252 between the profiles of SIPS by MG132 and BAFA1. For instance, the levels of SA-β-gal activity,
253 NRF1 and NRF2 induction, and mitochondrial biogenesis are relatively low in BAFA1-treated cells.
254 In addition, the overall SIPS progression in BAFA1-treated cells seems to be slower than that
255 observed in MG132-treated cells. Therefore, we could not exclude the occurrence of drug-specific
256 induction mechanisms in our SIPS model.

257 Mitochondria are considered to be the main source of ROS generated in cells.
258 Dysfunctional mitochondria that show decreased membrane potential and excess mitochondrial ROS
259 accumulate in senescent cells [21, 34]. It has also been established that the mitochondrial mass [20,
260 35] and OXPHOS activity [25] increase during cellular senescence. Thus, mitochondrial function
261 and metabolism are the major determinants of cellular aging [19]. Based on our results, it is likely
262 that there are two phases of mitochondrial status in which mitochondrial membrane potential only
263 temporarily decreased during MG132 or BAFA1 treatment, but significantly increased thereafter
264 (Fig. 3B) along with a significant increase in mitochondrial mass (Fig. 3A and 3D) and ATP levels

bioRxiv preprint doi: https://doi.org/10.1101/2020.01.22.916221; this version posted January 30, 2020. The copyright holder for this preprint (which was not certified by peer review) is the author/funder, who has granted bioRxiv a license to display the preprint in perpetuity. It is made available under aCC-BY-ND 4.0 International license.

265 (Fig. 3E), suggesting an increase in functional mitochondria during the latter period of SIPS
266 progression. Enhanced mitochondrial biogenesis was confirmed by notable increase in PGC-1α and
267 TFAM proteins (Fig. 3F) that were critically involved in mitochondrial biogenesis, whereas Parkin
268 (Fig. 3F) and LC3-II (Fig. 1G) were greatly downregulated, implying that mitophagic flux was
269 suppressed during enhanced mitochondrial biogenesis (day 5 to PD2). Furthermore, we observed
270 depletion of antioxidant enzymes in mitochondrial fraction (Fig. 4A) and aggresome-like inclusions
271 of SOD2 in the cytoplasm (Fig. 4B) as early as day 1, implying that nuclear-encoded antioxidant
272 proteins were insufficiently translocated into the mitochondria.

273 Rapamycin treatment partially attenuates cellular senescence induced by MG132 or
274 BAFA1 (Fig. 5B and 5C). Rapamycin treatment with MG132 or BAFA1 during days 0-5 (Rapa1)
275 significantly suppressed intracellular H_2O_2 (Fig. 5D and 5E), mitochondrial ROS production (Fig.
276 5G), and mitochondrial biogenesis (Fig. 5F) compared with cells treated with only MG132 or
277 BAFA1. The suppression of ROS by rapamycin could be partly because of enhanced upregulation of
278 overall and mitochondrial levels of SOD2 (Fig. 5H, BAFA1) and GPx4 (Fig. 5H, MG132). We also
279 found that co-treatment with NAC during days 1 and 2 (NAC1) significantly inhibited mitochondrial
280 biogenesis (Fig. 6B). Taken together, it is likely that rapamycin attenuates MG132- or

bioRxiv preprint doi: https://doi.org/10.1101/2020.01.22.916221; this version posted January 30, 2020. The copyright holder for this preprint (which was not certified by peer review) is the author/funder, who has granted bioRxiv a license to display the preprint in perpetuity. It is made available under aCC-BY-ND 4.0 International license.

BAFA1-induced SIPS by repressing an initial increase in intracellular and mitochondrial ROS levels and the following mitochondrial biogenesis. On the contrary, immunoblot analyses revealed that an induction level of PGC-1α was not altered by co-treatment with rapamycin compared to cells without rapamycin (Fig. S6). Notably, an active form of LC3, LC3-II, was not upregulated by rapamycin co-treatment (Fig. S6), implying that autophagic flux for damaged mitochondrial clearance does not contribute to rapamycin effect on SIPS. Thus, further investigation is required to clarify the detailed molecular link between suppression of ROS and mitochondrial biogenesis by rapamycin co-treatment.

Proteolytic activities and rate of protein turnover decline in aged organisms, which result in intracellular accumulation of insoluble protein aggregates. Whether age-related accumulation of protein aggregates is the determinant of cellular senescence or a characteristic product in aged cells still remains controversial. What is the link between protein aggregates observed in our SIPS model and cellular senescence? We found that aggregated proteins accumulated from day 1 by treatment with MG132 or BAFA1 (Fig. 1E). Overloading of increased aggregates may impair another proteolytic system that is not inhibited by the drug, which changes the cytosolic environment to accelerate widespread protein aggregation. Although we did not completely demonstrated that

bioRxiv preprint doi: https://doi.org/10.1101/2020.01.22.916221; this version posted January 30, 2020. The copyright holder for this preprint (which was not certified by peer review) is the author/funder, who has granted bioRxiv a license to display the preprint in perpetuity. It is made available under aCC-BY-ND 4.0 International license.

297 mitochondrial antioxidant enzymes, SOD2 and PGx4, form aggregations and are unable to
298 translocate to the mitochondria, temporal reduction of these proteins in mitochondrial fraction (Fig.
299 4A) may reflect the proteostasis stresses caused by protein aggregates. At the final stage of SIPS
300 induction, protein aggregates were still detectable even at PD6 (Fig. 1E); nevertheless, proteasome
301 activity and lysosome acidity have recovered at PD5 (data not shown), suggesting impaired protein
302 clearance in senescent cells. Thus, it is likely that aggregated proteins accumulated at the late stage
303 of senescence induction could be resistant to proteolysis by proteasome or lysosome. For the reason
304 that we did not find autofluorescent pigments in any stage of SIPS cells, the aggresome-like particles
305 that we observed might have different properties from those of lipofuscin. Artificial
306 lipofuscin-loaded human fibroblast showed aged morphology [36]. To conclude whether these
307 aggregated inclusion bodies could be a causal factor in SIPS by prolonged disturbance of
308 proteostasis or not, we are, at present, analyzing the nature of the aggregates such as protein
309 modification like carbonylation and ubiquitination, and phenotypes of these aggresome-induced
310 cells.

311 In conclusion, disturbance of proteostasis changes distribution of nuclear-encoded
312 mitochondrial antioxidant proteins at an early period of treatment, which enhances mitochondrial

bioRxiv preprint doi: https://doi.org/10.1101/2020.01.22.916221; this version posted January 30, 2020. The copyright holder for this preprint (which was not certified by peer review) is the author/funder, who has granted bioRxiv a license to display the preprint in perpetuity. It is made available under aCC-BY-ND 4.0 International license.

ROS production and temporal mitochondrial dysfunction. ROS in turn activates stress responses including NRF1/2 and AMPK pathways, followed by PGC-1α-mediated mitochondrial biogenesis. During the mid-stage of SIPS progression, excessive ROS is continuously generated from increased mitochondria, which can cause further cumulative damage to nuclear DNA and cell cycle arrest, and eventually lead to cellular senescence (Fig. 7).

Materials and methods

Reagents

MG132 and BAFA1 were purchased from ChemScene (Monmouth Junction, NJ) and Sigma-Aldrich (St. Louis, MO), respectively. Diaminofluorescein-FM diacetate (DAF-FM), OxiORANGE, and HYDROP were from Goryo Chemical (Sapporo, Japan). *N*-Acetyl-L-cysteine was from Fujifilm Wako Pure Chemical Corp (Osaka, Japan). Rapamycin was from LC Laboratories (Woburn, MA).

Cell culture

MRC-5 cells (30 PDL) were obtained from JCRB Cell Bank. Cells were maintained in EMEM (Fujifilm Wako Pure Chemical Corp, Osaka, Japan) supplemented with 10% fetal bovine serum

bioRxiv preprint doi: https://doi.org/10.1101/2020.01.22.916221; this version posted January 30, 2020. The copyright holder for this preprint (which was not certified by peer review) is the author/funder, who has granted bioRxiv a license to display the preprint in perpetuity. It is made available under aCC-BY-ND 4.0 International license.

329 (Biological Industries, Cromwell, CT) and penicillin-streptomycin (Nacalai tesque, Kyoto, Japan) at

330 37°C in a humidified atmosphere of 5% CO_2. Cells were passaged every 2 days.

331

332 **Cell growth assay**

333 For MG132 or BAFA1 treatment, we plated 1×10^4 cells a well in a 96-well clear bottom black plate,

334 allowed them to grow for 16-24 h, and then changed the culture medium to EMEM that contained

335 MG132 or BAFA1. As a pilot experiment, we assessed the viability of cells treated with MG132

336 (0.1-1 μM) or BAFA1 (2-15 nM) at several different concentrations to determine the appropriate

337 concentration of each drug. On day 5 of drug treatment, the culture medium was replaced with

338 regular EMEM that contained no drug.

339

340 **Immunoblotting and antibodies**

341 Cells cultured in 6-cm dishes were trypsinized and harvested. Cell pellets were lysed in modified

342 RIPA buffer (20 mM Tris-HCl, pH7.4, 50 mM NaCl, 0.5% Nonidet P-40, 0.05% sodium dodecyl

343 sulfate (SDS), 1 mM EDTA). Protein concentration was determined using Quick Start Bradford dye

344 (Bio-Rad, Hercules, CA). Whole cell extracts (10-15 μg) were mixed with 5×SDS sample buffer

bioRxiv preprint doi: https://doi.org/10.1101/2020.01.22.916221; this version posted January 30, 2020. The copyright holder for this preprint (which was not certified by peer review) is the author/funder, who has granted bioRxiv a license to display the preprint in perpetuity. It is made available under aCC-BY-ND 4.0 International license.

345 containing 2-mercaptoethanol, heated at 95°C for 3 min, and then loaded onto a
346 SDS-polyacrylamide gel. Proteins were transferred to a PVDF membrane and incubated in 1%
347 Western blocking reagent (Sigma-aldrich, St. Louis, MO) at 25°C for 1 hr. The membrane was then
348 incubated overnight with antibodies diluted in 0.5% Western blocking reagent. Antibodies used in
349 this study are summarized in a supplemental file. HRP-conjugated goat anti-mouse IgG
350 (Sigma-Aldrich) or anti-rabbit IgG (GE healthcare, Piscataway, NJ) antibodies were used as the
351 secondary antibodies and detected with ECL prime reagent (GE Healthcare). The
352 chemiluminescence signal was imaged by LAS4000 (GE Healthcare).
353

354 **SA-β-gal staining and senescence assays**

355 SA-β-gal staining was performed as described previously [9]. Quantitation of SA-β-gal activity was
356 assessed using a Cellular Senescence Plate Assay Kit - SPiDER-βGal (Dojindo, Kumamoto, Japan),
357 following the manufacturer's instructions.
358

359 **Immunofluorescence**

360 For immunofluorescence analyses of γH2A.X and SOD2, cells were fixed in 4%

bioRxiv preprint doi: https://doi.org/10.1101/2020.01.22.916221; this version posted January 30, 2020. The copyright holder for this preprint (which was not certified by peer review) is the author/funder, who has granted bioRxiv a license to display the preprint in perpetuity. It is made available under aCC-BY-ND 4.0 International license.

361 paraformaldehyde/PBS, treated with 0.5% Triton X-100/PBS for 10 min, incubated in Blocking One
362 Histo (Nacalai tesque) for 1 h, and incubated with diluted primary antibody overnight. After several
363 PBS washes, cells were incubated with a secondary antibody conjugated to DyLight 488 (Cosmo
364 Bio Co., Ltd., Tokyo, Japan) and Hoechst 33342, and observed under a fluorescence microscope
365 IX83 (Olympus, Tokyo, Japan) using appropriate filter sets.
366

367 **Measurement of ROS and NO**

368 Production of hydroxyl radical (·OH) and hypochlorous acid (HClO) was measured using
369 OxiORANGE reagent (Goryo Chemical). H_2O_2 and NO were detected by HYDROP and
370 diaminofluorescein-FM diacetate (DAF-FM DA, Goryo Chemical), respectively. Cells plated in a
371 96-well Black IsoPlate (PerkinElmer, Waltham, MA) were incubated with 0.5 μM OxiORANGE, 1
372 μM HYDROP or 1 μM DAF-FM DA diluted in EMEM containing FBS for 30 min at 37°C, and
373 then washed with 100 μl HBSS once. Fluorescence (Ex/Em = 535/595 nm for OxiORANGE,
374 485/535 nm for HYDROP and DAF-FM DA) was measured by FilterMax F5 (Molecular Devices,
375 San Jose, CA). Normalized values were obtained by dividing fluorescent intensities of HYDROP
376 and DAF-FM DA by protein concentration or dividing the fluorescent intensities of of OxiORANGE

bioRxiv preprint doi: https://doi.org/10.1101/2020.01.22.916221; this version posted January 30, 2020. The copyright holder for this preprint (which was not certified by peer review) is the author/funder, who has granted bioRxiv a license to display the preprint in perpetuity. It is made available under aCC-BY-ND 4.0 International license.

by nuclear fluorescent signal stained with Hoechst 33342 (Dojindo).

Staining of protein aggregation

Protein aggregation was visualized by Proteostat Aggresome Detection Reagent (Enzo Life Science, Farmingdale, NY), according to the manufacturer's protocol. For the quantitative analysis, cells plated in 96-well black plates were fixed with 2% PFA, permeabilized with 0.5% Triton X-100, and stained with Proteostat Aggresome Detection Reagent diluted in EMEM containing FBS at 1:2,000 for 30 min at 25°C, then fluorescence was measured (Ex/Em = 485/595 nm) using FilterMax F5 (Molecular Devices).

Intracellular ATP assay

Intracellular ATP levels were measured using "Cell" ATP Assay reagent (Toyo B-Net, Tokyo, Japan). The ATP level was normalized by the DNA content in cell lysates, which was quantified by SYBR Gold stain (Thermo Fisher Scientific, Waltham, MA).

Preparation of mitochondrial fraction

bioRxiv preprint doi: https://doi.org/10.1101/2020.01.22.916221; this version posted January 30, 2020. The copyright holder for this preprint (which was not certified by peer review) is the author/funder, who has granted bioRxiv a license to display the preprint in perpetuity. It is made available under aCC-BY-ND 4.0 International license.

The procedure for isolation of mitochondrial fraction from cultured cells is as described by Clayton *et al* [37] with slight modifications. The buffer volume, number of strokes, homogenizer, and pestle used were optimized for 0.5-1.0 × 10^6 cells. Frozen cell pellets were resuspended in hypotonic buffer and homogenized using a disposable plastic pestle (As One Corp., Osaka, Japan) with matched Safe-Lock tubes (Eppendorf, Hamburg, Germany). The detailed procedure is summarized in Fig. S4A-C.

Live cell microscopy for mitochondrial analyses

For the detection of mitochondrial mass and ΔΨm, live cells were incubated with 0.5 μM MitoTracker Green FM (Thermo Fisher Scientific) and 0.5 μM MitoTracker Red CM-H2Xros (Thermo Fisher Scientific) with 2 μg/mL Hoechst 33342 diluted in EMEM containing FBS for 30 min at 37°C, and then washed with 100 μl HBSS once. For the detection of mitochondrial ROS, cells were incubated with 5 μM MitoSOX Red mitochondrial superoxide indicator (Thermo Fisher Scientific) in HBSS for 10 min at 37°C, washed with HBSS 3 times, and cultured in regular medium for 24 h. On the next day, cells were stained with Hoechst 33342, washed with 100 μl HBSS once, and observed under an all-in-one fluorescence microscope BZ-9000 (Keyence, Osaka, Japan) using appropriate filter sets. Fluorescence images were analyzed and quantified using ImageJ software ver.

bioRxiv preprint doi: https://doi.org/10.1101/2020.01.22.916221; this version posted January 30, 2020. The copyright holder for this preprint (which was not certified by peer review) is the author/funder, who has granted bioRxiv a license to display the preprint in perpetuity. It is made available under aCC-BY-ND 4.0 International license.

2.0.0.

Statistical analyses

We conducted one-way ANOVA followed by Tukey's multiple comparison test. Two groups were compared using a non-parametric Mann-Whitney *U* test. Differences between groups with a *p* value of <0.05 were considered significant. All data were analyzed using GraphPad Prism 5.0 software and presented as mean ± SD of the obtained values.

Acknowledgement

We are grateful to Santa Cruz Biotechnology, Inc. (Dallas, Tx) and Cosmo Bio Co., Ltd. (Tokyo, Japan) for providing sample antibodies listed in Antibodies used in this study. We would like to thank Editage (www.editage.jp) for English language editing.

AUTHOR CONTRIBUTIONS

Y. T. and Y. K. designed the research and drafted the paper; Y. T. carried out experiments and analyzed data; and I. I., T. N., and M. I. supported analysis of oxidative stress.

bioRxiv preprint doi: https://doi.org/10.1101/2020.01.22.916221; this version posted January 30, 2020. The copyright holder for this preprint (which was not certified by peer review) is the author/funder, who has granted bioRxiv a license to display the preprint in perpetuity. It is made available under aCC-BY-ND 4.0 International license.

FUNDING INFO

This work was supported by a Nippon Medical School Grant-in-Aid for Medical Research 2019.

CONFLICT OF INTEREST

The authors have no conflicts of interest to declare in association with this study.

REFERENCES

1. Hayashi, T. & Goto, S. (1998) Age-related changes in the 20S and 26S proteasome activities in the liver of male F344 rats, *Mech Ageing Dev*. **102**, 55-66.

2. Ishigami, A. & Goto, S. (1990) Age-related change in the degradation rate of ovalbumin microinjected into mouse liver parenchymal cells, *Arch Biochem Biophys*. **277**, 189-95.

3. Hwang, J. S., Hwang, J. S., Chang, I. & Kim, S. (2007) Age-associated decrease in proteasome content and activities in human dermal fibroblasts: restoration of normal level of proteasome subunits reduces aging markers in fibroblasts from elderly persons, *J Gerontol A Biol Sci Med Sci*. **62**, 490-9.

4. Reeg, S. & Grune, T. (2015) Protein Oxidation in Aging: Does It Play a Role in Aging Progression?,

bioRxiv preprint doi: https://doi.org/10.1101/2020.01.22.916221; this version posted January 30, 2020. The copyright holder for this preprint (which was not certified by peer review) is the author/funder, who has granted bioRxiv a license to display the preprint in perpetuity. It is made available under aCC-BY-ND 4.0 International license.

Antioxid Redox Signal. **23**, 239-55.

5. Hohn, A. & Grune, T. (2013) Lipofuscin: formation, effects and role of macroautophagy, *Redox Biol*. **1**, 140-4.

6. Chang, B. D., Watanabe, K., Broude, E. V., Fang, J., Poole, J. C., Kalinichenko, T. V. & Roninson, I. B. (2000) Effects of p21Waf1/Cip1/Sdi1 on cellular gene expression: implications for carcinogenesis, senescence, and age-related diseases, *Proc Natl Acad Sci U S A*. **97**, 4291-6.

7. Hasty, P., Sharp, Z. D., Curiel, T. J. & Campisi, J. (2013) mTORC1 and p53: clash of the gods?, *Cell Cycle*. **12**, 20-5.

8. Leontieva, O. V., Gudkov, A. V. & Blagosklonny, M. V. (2010) Weak p53 permits senescence during cell cycle arrest, *Cell Cycle*. **9**, 4323-7.

9. Dimri, G., Lee, X., Basile, G., Acosta, M., Scott, G., Roskelley, C., Medrano, E., Linskens, M., Rubelj, I. & Pereira-Smith, O. (1995) A biomarker that identifies senescent human cells in culture and in aging skin in vivo, *Proc Natl Acad Sci U S A*. **92**, 9363-7.

10. Maejima, Y., Adachi, S., Ito, H., Hirao, K. & Isobe, M. (2008) Induction of premature senescence in cardiomyocytes by doxorubicin as a novel mechanism of myocardial damage, *Aging Cell*. **7**, 125-36.

11. Moiseeva, O., Bourdeau, V., Roux, A., Deschenes-Simard, X. & Ferbeyre, G. (2009) Mitochondrial

bioRxiv preprint doi: https://doi.org/10.1101/2020.01.22.916221; this version posted January 30, 2020. The copyright holder for this preprint (which was not certified by peer review) is the author/funder, who has granted bioRxiv a license to display the preprint in perpetuity. It is made available under aCC-BY-ND 4.0 International license.

457 dysfunction contributes to oncogene-induced senescence, *Mol Cell Biol*. **29**, 4495-507.

458 12. Park, W. H. & Kim, S. H. (2012) MG132, a proteasome inhibitor, induces human pulmonary

459 fibroblast cell death via increasing ROS levels and GSH depletion, *Oncol Rep*. **27**, 1284-91.

460 13. Maharjan, S., Oku, M., Tsuda, M., Hoseki, J. & Sakai, Y. (2014) Mitochondrial impairment triggers

461 cytosolic oxidative stress and cell death following proteasome inhibition, *Sci Rep*. **4**, 5896.

462 14. Chao, T. H., Chang, M. Y., Su, S. J. & Su, S. H. (2014) Inducible nitric oxide synthase mediates

463 MG132 lethality in leukemic cells through mitochondrial depolarization, *Free Radic Biol Med*. **74**,

464 175-87.

465 15. Chondrogianni, N. & Gonos, E. S. (2004) Proteasome inhibition induces a senescence-like

466 phenotype in primary human fibroblasts cultures, *Biogerontology*. **5**, 55-61.

467 16. Chondrogianni, N., Stratford, F. L., Trougakos, I. P., Friguet, B., Rivett, A. J. & Gonos, E. S. (2003)

468 Central role of the proteasome in senescence and survival of human fibroblasts: induction of a

469 senescence-like phenotype upon its inhibition and resistance to stress upon its activation, *J Biol Chem*.

470 **278**, 28026-37.

471 17. Ukekawa, R., Maegawa, N., Mizutani, E., Fujii, M. & Ayusawa, D. (2004) Proteasome inhibitors

472 induce changes in chromatin structure characteristic of senescent human fibroblasts, *Biosci Biotechnol*

bioRxiv preprint doi: https://doi.org/10.1101/2020.01.22.916221; this version posted January 30, 2020. The copyright holder for this preprint (which was not certified by peer review) is the author/funder, who has granted bioRxiv a license to display the preprint in perpetuity. It is made available under aCC-BY-ND 4.0 International license.

Biochem. **68**, 2395-7.

18. Brand, M. D. (2016) Mitochondrial generation of superoxide and hydrogen peroxide as the source of mitochondrial redox signaling, *Free Radic Biol Med*. **100**, 14-31.

19. Wei, Y., Zhang, Y. J., Cai, Y. & Xu, M. H. (2015) The role of mitochondria in mTOR-regulated longevity, *Biol Rev Camb Philos Soc*. **90**, 167-81.

20. Lee, H. C., Yin, P. H., Chi, C. W. & Wei, Y. H. (2002) Increase in mitochondrial mass in human fibroblasts under oxidative stress and during replicative cell senescence, *J Biomed Sci*. **9**, 517-26.

21. Passos, J. F., Nelson, G., Wang, C., Richter, T., Simillion, C., Proctor, C. J., Miwa, S., Olijslagers, S., Hallinan, J., Wipat, A., Saretzki, G., Rudolph, K. L., Kirkwood, T. B. & von Zglinicki, T. (2010) Feedback between p21 and reactive oxygen production is necessary for cell senescence, *Mol Syst Biol*. **6**, 347.

22. Huss, M. & Wieczorek, H. (2009) Inhibitors of V-ATPases: old and new players, *J Exp Biol*. **212**, 341-6.

23. Cho, S. & Hwang, E. S. (2012) Status of mTOR activity may phenotypically differentiate senescence and quiescence, *Mol Cells*. **33**, 597-604.

24. Blagosklonny, M. V. (2011) Cell cycle arrest is not senescence, *Aging (Albany NY)*. **3**, 94-101.

bioRxiv preprint doi: https://doi.org/10.1101/2020.01.22.916221; this version posted January 30, 2020. The copyright holder for this preprint (which was not certified by peer review) is the author/funder, who has granted bioRxiv a license to display the preprint in perpetuity. It is made available under aCC-BY-ND 4.0 International license.

25. Takebayashi, S., Tanaka, H., Hino, S., Nakatsu, Y., Igata, T., Sakamoto, A., Narita, M. & Nakao, M. (2015) Retinoblastoma protein promotes oxidative phosphorylation through upregulation of glycolytic genes in oncogene-induced senescent cells, *Aging Cell*. **14**, 689-97.

26. Legesse-Miller, A., Raitman, I., Haley, E. M., Liao, A., Sun, L. L., Wang, D. J., Krishnan, N., Lemons, J. M., Suh, E. J., Johnson, E. L., Lund, B. A. & Coller, H. A. (2012) Quiescent fibroblasts are protected from proteasome inhibition-mediated toxicity, *Mol Biol Cell*. **23**, 3566-81.

27. Rawat, S., Anusha, V., Jha, M., Sreedurgalakshmi, K. & Raychaudhuri, S. (2019) Aggregation of Respiratory Complex Subunits Marks the Onset of Proteotoxicity in Proteasome Inhibited Cells, *J Mol Biol*. **431**, 996-1015.

28. Morita, M., Gravel, S. P., Hulea, L., Larsson, O., Pollak, M., St-Pierre, J. & Topisirovic, I. (2015) mTOR coordinates protein synthesis, mitochondrial activity and proliferation, *Cell Cycle*. **14**, 473-80.

29. Ramanathan, A. & Schreiber, S. L. (2009) Direct control of mitochondrial function by mTOR, *Proc Natl Acad Sci U S A*. **106**, 22229-32.

30. Martinez-Cisuelo, V., Gomez, J., Garcia-Junceda, I., Naudi, A., Cabre, R., Mota-Martorell, N., Lopez-Torres, M., Gonzalez-Sanchez, M., Pamplona, R. & Barja, G. (2016) Rapamycin reverses age-related increases in mitochondrial ROS production at complex I, oxidative stress, accumulation of

bioRxiv preprint doi: https://doi.org/10.1101/2020.01.22.916221; this version posted January 30, 2020. The copyright holder for this preprint (which was not certified by peer review) is the author/funder, who has granted bioRxiv a license to display the preprint in perpetuity. It is made available under aCC-BY-ND 4.0 International license.

505 mtDNA fragments inside nuclear DNA, and lipofuscin level, and increases autophagy, in the liver of
506 middle-aged mice, *Exp Gerontol*. **83**, 130-8.

507 31. Summer, R., Shaghaghi, H., Schriner, D., Roque, W., Sales, D., Cuevas-Mora, K., Desai, V.,
508 Bhushan, A., Ramirez, M. I. & Romero, F. (2019) Activation of the mTORC1/PGC-1 axis promotes
509 mitochondrial biogenesis and induces cellular senescence in the lung epithelium, *Am J Physiol Lung Cell*
510 *Mol Physiol*. **316**, L1049-L1060.

511 32. Leontieva, O. V., Demidenko, Z. N., Gudkov, A. V. & Blagosklonny, M. V. (2011) Elimination of
512 proliferating cells unmasks the shift from senescence to quiescence caused by rapamycin, *PLoS One*. **6**,
513 e26126.

514 33. Lerner, C., Bitto, A., Pulliam, D., Nacarelli, T., Konigsberg, M., Van Remmen, H., Torres, C. &
515 Sell, C. (2013) Reduced mammalian target of rapamycin activity facilitates mitochondrial retrograde
516 signaling and increases life span in normal human fibroblasts, *Aging Cell*. **12**, 966-77.

517 34. Nacarelli, T. & Sell, C. (2017) Targeting metabolism in cellular senescence, a role for intervention,
518 *Mol Cell Endocrinol*. **455**, 83-92.

519 35. Korolchuk, V. I., Miwa, S., Carroll, B. & von Zglinicki, T. (2017) Mitochondria in Cell Senescence:
520 Is Mitophagy the Weakest Link?, *EBioMedicine*. **21**, 7-13.

bioRxiv preprint doi: https://doi.org/10.1101/2020.01.22.916221; this version posted January 30, 2020. The copyright holder for this preprint (which was not certified by peer review) is the author/funder, who has granted bioRxiv a license to display the preprint in perpetuity. It is made available under aCC-BY-ND 4.0 International license.

36. Nilsson, E. & Yin, D. (1997) Preparation of artificial ceroid/lipofuscin by UV-oxidation of subcellular organelles, *Mech Ageing Dev*. **99**, 61-78.

37. Clayton, D. A. & Shadel, G. S. (2014) Isolation of mitochondria from tissue culture cells, *Cold Spring Harb Protoc*. **2014**, pdb prot080002.

Figure legends

Fig. 1

Prolonged disturbance of proteostasis by MG132 or BAFA1 induces premature senescence in normal human fibroblasts. (A) The experimental design to induce SIPS in MRC-5 by MG132 or BAFA1. MRC-5 cells (37-40 PDL) were treated with 0.1-1 μM MG132 or 2-15 nM BAFA1 consecutively for 3 or 5 days without medium refreshment. On day 3 or 5, the drugs were removed and cells were kept in regular culture medium for additional 5 days. Day, days during the drug treatment; PD, post-treatment days. (B) Cell proliferation was monitored by measuring Hoechst 33342 fluorescence from PD1 to PD6. Cells were treated with MG132 or BAFA1 for 3 or 5 days, and then cultured in medium without the drug for 6 days (PD1-6). Values are shown as mean ± SD from 4 wells of a 96-well plate. The asterisk (*) indicates $p < 0.05$ by one-way ANOVA, followed by Tukey's multiple comparison test for PD1 vs. others. (C) Representative pictures of

bioRxiv preprint doi: https://doi.org/10.1101/2020.01.22.916221; this version posted January 30, 2020. The copyright holder for this preprint (which was not certified by peer review) is the author/funder, who has granted bioRxiv a license to display the preprint in perpetuity. It is made available under aCC-BY-ND 4.0 International license.

538 SA-β-gal-positive MRC-5 cells. Cells were treated with MG132 or BAFA1 for 3 or 5 days,
539 respectively, and stained at PD7 (cytoplasmic blue precipitate). Control, untreated young (39 PDL)
540 and old (59 PDL) MRC-5 cells undergoing replicative senescence. (D) SA-β-gal activity was
541 measured using a SPiDER-βGal Cellular Senescence Plate Assay Kit. Fluorescence signal derived
542 from SA-β-gal was normalized by Hoechst 33342-stained nuclear signal. C, untreated control cells.
543 Values are shown as mean ± SD from 4 wells of a 96-well plate. The asterisk (*) indicates $p < 0.05$
544 by one-way ANOVA, followed by Tukey's multiple comparison test for control vs. treated cells. (E)
545 Representative images of accumulation of aggresome-like inclusion bodies in senescence-induced
546 MRC-5 cells. Cells were treated with MG132 or BAFA1 for 5 days, respectively, and stained with
547 Proteostat Aggresome detection reagent (red) and Hoechst 33342 (blue). Scale bar = 50 μm. (F)
548 Representative images of control and MG132- or BAFA1-treated MRC-5 cells immunostained for
549 γH2A.X (green) and Hoechst 33342 (blue). Scale bar = 50 μm. (G) Immunoblot analyses for CDK
550 inhibitor p21, p53, DNA damage response marker γH2A.X, downstream target of mTORC1 S6 and
551 phosphorylated $S6^{Thr235/236}$, autophagy marker LC3, and GAPDH from control and MG132- or
552 BAFA1-treated MRC-5 cells. (H) Immunoblot analyses for NRF1 and NRF2 from control and
553 MG132- or BAFA1-treated MRC-5 cells.

bioRxiv preprint doi: https://doi.org/10.1101/2020.01.22.916221; this version posted January 30, 2020. The copyright holder for this preprint (which was not certified by peer review) is the author/funder, who has granted bioRxiv a license to display the preprint in perpetuity. It is made available under aCC-BY-ND 4.0 International license.

Fig. 2

Prolonged disturbance of proteostasis by MG132 or BAFA1 enhances ROS production. (A) Quantitation of relative intracellular ROS levels using OxiORANGE reagent that selectively detects hydroxyl radical (·OH) and hypochlorous acid (HClO). The fluorescence intensity for OxiORANGE (Ex/Em = 535/595) was normalized by Hoechst 33342 intensity (Ex/Em = 340/465). Values are shown as mean ± SD from 4 wells of a 96-well plate. The asterisk (*) indicates $p < 0.05$ by one-way ANOVA, followed by Tukey's multiple comparison test for control vs. treated cells. (B) Representative images of control and MG132- or BAFA1-treated (PD1) MRC-5 cells stained for the OxiORANGE (red) and Hoechst 33342 (blue). Scale bar = 50 μm. (C) Quantitation of relative intracellular H_2O_2 levels using HYDROP reagent that selectively detects H_2O_2. The fluorescence intensity for HYDROP was normalized by total protein concentration. Values are shown as mean ± SD from 4 wells of a 96-well plate. (D) Representative images of control and MG132- or BAFA1-treated (PD1) MRC-5 cells stained for the HYDROP (green) and Hoechst 33342 (blue). Scale bar = 50 μm. (E) Relative mitochondrial ROS levels were monitored using a MitoSOX Red mitochondrial superoxide indicator. The fluorescence intensities for MitoSOX and Hoechst 33342

bioRxiv preprint doi: https://doi.org/10.1101/2020.01.22.916221; this version posted January 30, 2020. The copyright holder for this preprint (which was not certified by peer review) is the author/funder, who has granted bioRxiv a license to display the preprint in perpetuity. It is made available under aCC-BY-ND 4.0 International license.

570 were quantified by image analysis. MitoSOX intensity was normalized by the number of nuclei.
571 Values are shown as mean ± SD from the measurements of 4 different images. The asterisk (*)
572 indicates $p < 0.05$ by one-way ANOVA, followed by Tukey's multiple comparison test for control
573 vs. treated cells. Values obtained from cells treated with MG132 or BAFA1 on day 1 were compared
574 with those from untreated control cells using a non-parametric Mann-Whitney *U* test. The sharp (#)
575 indicates significant difference ($p < 0.05$). (F) Representative images of control and MG132- or
576 BAFA1-treated (PD3) MRC-5 cells stained for MitoSOX (red) and Hoechst 33342 (blue).
577
578 **Fig. 3**
579 Prolonged disturbance of proteostasis by MG132 or BAFA1 induces temporal mitochondrial
580 dysfunction and sequential mitochondrial biogenesis. (A) Relative mitochondrial mass was
581 monitored using MitoTracker Green FM. The fluorescence intensities for MitoTracker Green and
582 Hoechst 33342 were quantified by image analysis. MitoTracker Green intensity was normalized by
583 the number of nuclei. Values are shown as mean ± SD from the measurements of 5 different images.
584 The asterisk (*) indicates $p < 0.05$ by one-way ANOVA, followed by Tukey's multiple comparison
585 test for control vs. treated cells. (B) Relative mitochondrial membrane potential ($\Delta\Psi m$) was

bioRxiv preprint doi: https://doi.org/10.1101/2020.01.22.916221; this version posted January 30, 2020. The copyright holder for this preprint (which was not certified by peer review) is the author/funder, who has granted bioRxiv a license to display the preprint in perpetuity. It is made available under aCC-BY-ND 4.0 International license.

586 monitored using MitoTracker Red CM-H_2XRos. The fluorescence intensities for MitoTracker Red
587 CM-H_2XRos and Hoechst 33342 were quantified by image analysis. MitoTracker Red CM-H_2XRos
588 intensity was normalized by the number of nuclei. Values are shown as mean ± SD from the
589 measurements of 10 different images. The asterisk (*) indicates $p < 0.05$ by one-way ANOVA
590 followed by Tukey's multiple comparison test for control vs. treated cells. (C) Representative
591 images of control and MG132- or BAFA1-treated (day 5 and PD1) MRC-5 cells stained for the
592 MitoTracker Green FM (Mt mass, green), MitoTracker Red CM-H_2XRos ($\Delta\Psi$m, Red) and Hoechst
593 33342 (blue). (D) The copy number of mitochondrial DNA of control and MG132- or
594 BAFA1-treated MRC-5 cells was measured by qPCR using mtDNA-specific primers and nuclear
595 DNA-specific primers as a reference. Values are mean ± SD of results obtained from 3-4
596 independent experiments. The asterisk (*) indicates $p < 0.05$ by one-way ANOVA, followed by
597 Tukey's multiple comparison test for control vs. treated cells. (E) Intracellular ATP contents were
598 measured using a firefly luciferase. The luminescence was normalized by cellular DNA
599 concentration quantified using SYBR Gold. Values are shown as mean ± SD from 4 wells of a
600 96-well plate. The asterisk (*) indicates $p < 0.05$ by one-way ANOVA, followed by Tukey's
601 multiple comparison test for control (37 PDL) vs. treated cells. (F) Immunoblot analyses for

bioRxiv preprint doi: https://doi.org/10.1101/2020.01.22.916221; this version posted January 30, 2020. The copyright holder for this preprint (which was not certified by peer review) is the author/funder, who has granted bioRxiv a license to display the preprint in perpetuity. It is made available under aCC-BY-ND 4.0 International license.

PGC-1α, TFAM, Parkin, AMPKα, phosphorylated AMPKα^{Thr172} (p-AMPKα), COX4 and GAPDH from control and MG132 (left)- or BAFA1 (right)-treated MRC-5 cells.

Fig. 4

Translocation of antioxidant enzymes to mitochondria is impaired in the early period of MG132 or BAFA1 treatment in MRC-5 cells. (A) Immunoblot analyses for mitochondrial antioxidant enzymes SOD2 and GPx4, NDUFS3, Tom40, and GAPDH from control and MG132 (left)- or BAFA1 (right)-treated MRC-5 cells. Mt, mitochondrial fraction; Whole, whole cellular extract. (B) Representative images of control and MG132- or BAFA1-treated MRC-5 cells on day 1 immunostained for SOD2 (green) and Hoechst 33342 (blue). Scale bar = 50 μm.

Fig. 5

Rapamycin attenuates cellular senescence induced by MG132 or BAFA1. (A) The experimental design for co-treatment of 10 nM rapamycin with MG132 or BAFA1 in MRC-5. Rapa1, cells were co-treated with rapamycin and either MG132 or BAFA1 from day 0 to day 5. Rapa2, cells were co-treated with rapamycin and either MG132 or BAFA1 from day 3 to day 5, and continuously

bioRxiv preprint doi: https://doi.org/10.1101/2020.01.22.916221; this version posted January 30, 2020. The copyright holder for this preprint (which was not certified by peer review) is the author/funder, who has granted bioRxiv a license to display the preprint in perpetuity. It is made available under aCC-BY-ND 4.0 International license.

618 cultured in regular medium containing rapamycin from day 5 to PD3. (B) Cell proliferation was
619 monitored by measuring Hoechst 33342 fluorescence from PD5 to PD10. Values are shown as mean
620 ± SD from 4 wells of a 96-well plate. (C) SA-β-gal activities of cells co-treated with rapamycin and
621 either MG132 or BAFA1 were measured on PD5 using a SPiDER-βGal Cellular Senescence Plate
622 Assay Kit. Normalized values are shown as mean ± SD from 4 wells of a 96-well plate. Values
623 obtained from cells treated with rapamycin and either MG132 or BAFA1 (Rapa1 and Rapa2) were
624 compared with those from cells treated with only MG132 or BAFA1 (-) using a non-parametric
625 Mann-Whitney *U* test. The asterisk (*) indicates significant difference ($p < 0.05$). (D, E) Intracellular
626 H_2O_2 levels of cells co-treated with rapamycin and either MG132 or BAFA1 were measured on day
627 3, day 5, and PD3 by HYDROP staining. Normalized values are shown as mean ± SD from 4 wells
628 of a 96-well plate. Two groups were compared using a non-parametric Mann-Whitney *U* test (*$p <$
629 0.05). (F) Relative mitochondrial mass of cells co-treated with rapamycin and either of MG132 or
630 BAFA1 was measured on PD1 (MG132) and PD2 (BAFA1) using MitoTracker Green FM. Values
631 are shown as mean ± SD from the measurements of 4 different images. Two groups were compared
632 using a non-parametric Mann-Whitney *U* test (*$p < 0.05$). (G) Relative mitochondrial ROS levels of
633 cells co-treated with rapamycin (+Rapa) and either of MG132 or BAFA1 were measured on day 1

bioRxiv preprint doi: https://doi.org/10.1101/2020.01.22.916221; this version posted January 30, 2020. The copyright holder for this preprint (which was not certified by peer review) is the author/funder, who has granted bioRxiv a license to display the preprint in perpetuity. It is made available under aCC-BY-ND 4.0 International license.

(MG132) and day 2 (BAFA1). The MitoSOX intensity was normalized by the number of nuclei. Values are shown as mean ± SD from the measurements of 4 different images. Two groups were compared using a non-parametric Mann-Whitney *U* test (*$p < 0.05$). (H) Immunoblot analyses for SOD2, GPx4, Tom40, and GAPDH from MG132- or BAFA1-treated cells with (+Rapa) or without (-Rapa) rapamycin on day 1. Mt, mitochondrial fraction; Whole, whole cellular extract.

Fig. 6

NAC attenuates an increase in mitochondrial mass induced by MG132 or BAFA1. (A) The experimental design for co-treatment of *N*-acetyl-L-cysteine (NAC) with MG132 or BAFA1 in MRC-5 cells. NAC1-3, cells were co-treated with 5 mM NAC and either of MG132 or BAFA1 from day 0 to day 2 (NAC1), day 2 to day 4 (NAC2), or day 5 to PD1 (NAC3, only NAC treatment during day 5 to PD1). (B) Relative mitochondrial mass of cells co-treated with NAC and either MG132 or BAFA1 was measured on PD1 (MG132) and PD2 (BAFA1) using MitoTracker Green FM. Values are shown as mean ± SD from the measurements of 6 different images. Two groups were compared using a non-parametric Mann-Whitney *U* test (*$p < 0.05$).

bioRxiv preprint doi: https://doi.org/10.1101/2020.01.22.916221; this version posted January 30, 2020. The copyright holder for this preprint (which was not certified by peer review) is the author/funder, who has granted bioRxiv a license to display the preprint in perpetuity. It is made available under aCC-BY-ND 4.0 International license.

Fig. 7

Speculative scheme of SIPS induced by MG132 or BAFA1. Upper panel shows mitochondrial events during SIPS progression induced by MG132 or BAFA1. Disturbance of proteostasis changes distribution of nuclear-encoded mitochondrial proteins including antioxidant enzymes SOD2 and GPx4 at a very early period of the treatment, which induces mitochondrial ROS and temporal mitochondrial dysfunction. ROS in turn activates stress response pathway including NRF1 and NRF2 upregulation, followed by PGC-1α-mediated mitochondrial biogenesis. During mid-stage of SIPS progression, excessive ROS was continuously generated from increased mitochondria, which could cause deleterious damage to nuclear DNA and cell cycle arrest, and eventually lead to cellular senescence. Lower panel summarizes kinetics of cellular outcomes including levels of SA-β-gal activity, DNA damage response, overall ROS, protein aggregation, and autophagic flux.

bioRxiv preprint doi: https://doi.org/10.1101/2020.01.22.916221; this version posted January 30, 2020. The copyright holder for this preprint (which was not certified by peer review) is the author/funder, who has granted bioRxiv a license to display the preprint in perpetuity. It is made available under aCC-BY-ND 4.0 International license.

Antibodies used in this study

1st antibodies

anti-p21 (SX118, sc-53870, Santa Cruz Biotechnology, mouse monoclonal)

anti-S6 (C-8, sc-74459, Santa Cruz Biotechnology, mouse monoclonal)

anti-p-S6 (50.Ser 235/236, sc-293144, Santa Cruz Biotechnology)

anti-p53 (DO-1, sc-126, Santa Cruz Biotechnology, mouse monoclonal)

anti-p-Histone H2A.X (Ser 139, sc-517348, Santa Cruz Biotechnology, mouse monoclonal)

anti-mtTFA (TFAM)(C-9, sc-376672, Santa Cruz Biotechnology, mouse monoclonal)

anti-PGC-1α (D-5, sc-518025, Santa Cruz Biotechnology, mouse monoclonal)

anti-Parkin (PRK8, sc-32282, Santa Cruz Biotechnology)

anti-SOD2 (A-2, sc-133134, Santa Cruz Biotechnology)

anti-GPx-4 (E-12, sc-166570, Santa Cruz Biotechnology, mouse monoclonal)

anti-NDUFS3 (D-4, sc-374282, Santa Cruz Biotechnology, mouse monoclonal)

anti-Tom40 (D-2, sc-365467, Santa Cruz Biotechnology, mouse monoclonal)

anti-NRF1 (G-5, sc-515360, Santa Cruz Biotechnology, mouse monoclonal)

anti-NRF2 (M200-3, Medical & Biological Laboratories Co., ltd., Japan, mouse monoclonal)

anti-Cox-4 (#3638-100, BioVision)

anti-LC3 (PM036, MBL Life Science)

anti-GAPDH (G8795, Sigma-aldrich)

anti-p-AMPKα (#2535, Cell Signaling Technology)

anti-AMPKα (#2532, Cell Signaling Technology)

2nd antibodies

HRP-conjugated goat anti-mouse IgG (A9044, Sigma-Aldrich)

HRP-conjugated anti-rabbit IgG (NA934, GE healthcare)

Luminescent signal detection

The luminescence signal by HRP on membrane was imaged with ECL prime reagent (GE Healthcare).

Figure 1

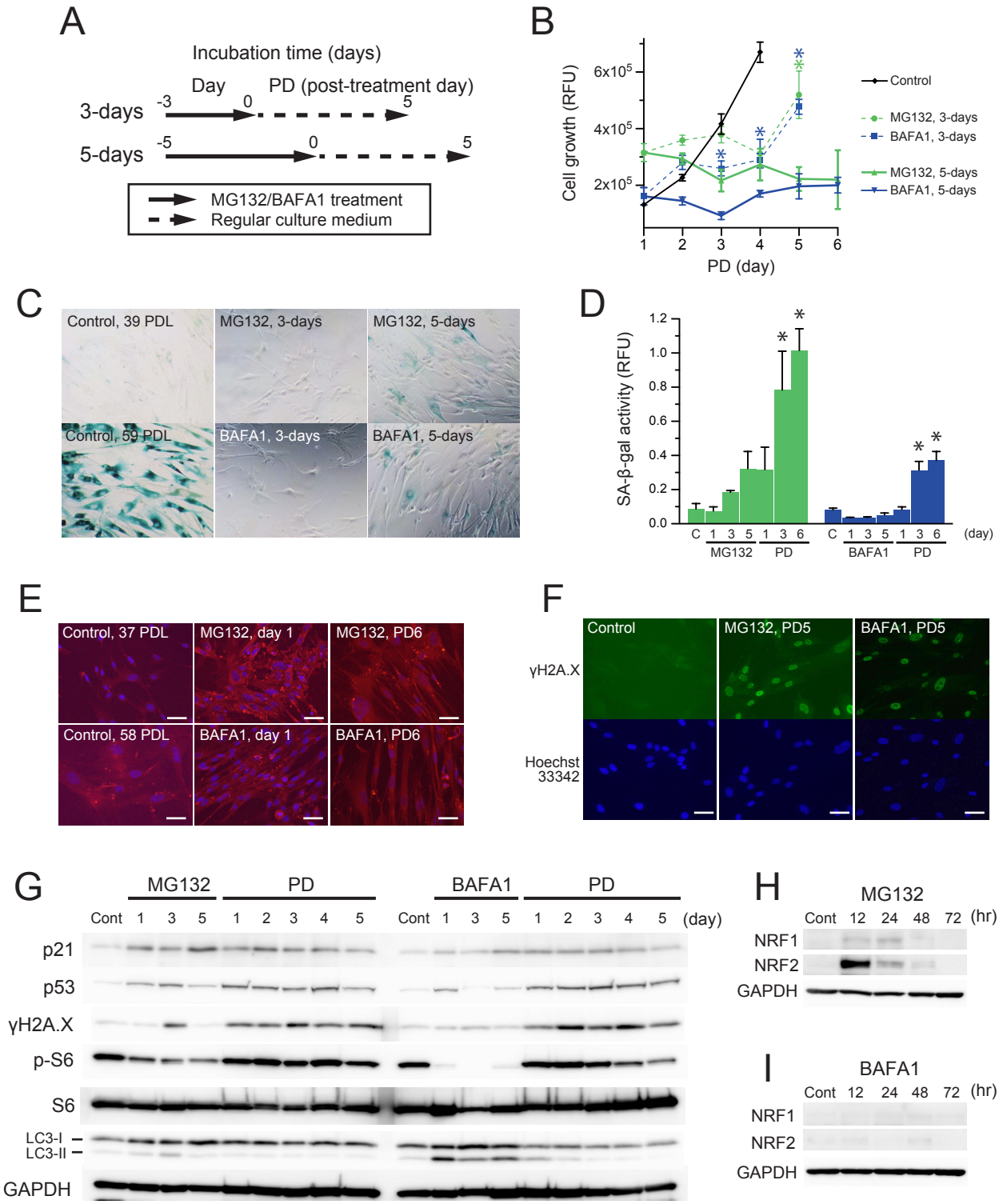
A
Incubation time (days)
Day
PD (post-treatment day)
3-days
-3
0
5
5-days
-5
0
5
MG132/BAFA1 treatment
Regular culture medium
B
Cell growth (RFU)
6x10^5
4x10^5
2x10^5
PD (day)
Control
MG132, 3-days
BAFA1, 3-days
MG132, 5-days
BAFA1, 5-days
C
Control, 39 PDL
MG132, 3-days
MG132, 5-days
Control, 59 PDL
BAFA1, 3-days
BAFA1, 5-days
D
SA-β-gal activity (RFU)
(day)
MG132
PD
BAFA1
PD
E
Control, 37 PDL
MG132, day 1
MG132, PD6
Control, 58 PDL
BAFA1, day 1
BAFA1, PD6
F
Control
MG132, PD5
BAFA1, PD5
γH2A.X
Hoechst 33342
G
MG132
PD
BAFA1
PD
Cont
(day)
p21
p53
γH2A.X
p-S6
S6
LC3-I
LC3-II
GAPDH
H
MG132
Cont
(hr)
NRF1
NRF2
GAPDH
I
BAFA1
Cont
(hr)
NRF1
NRF2
GAPDH

Figure 2

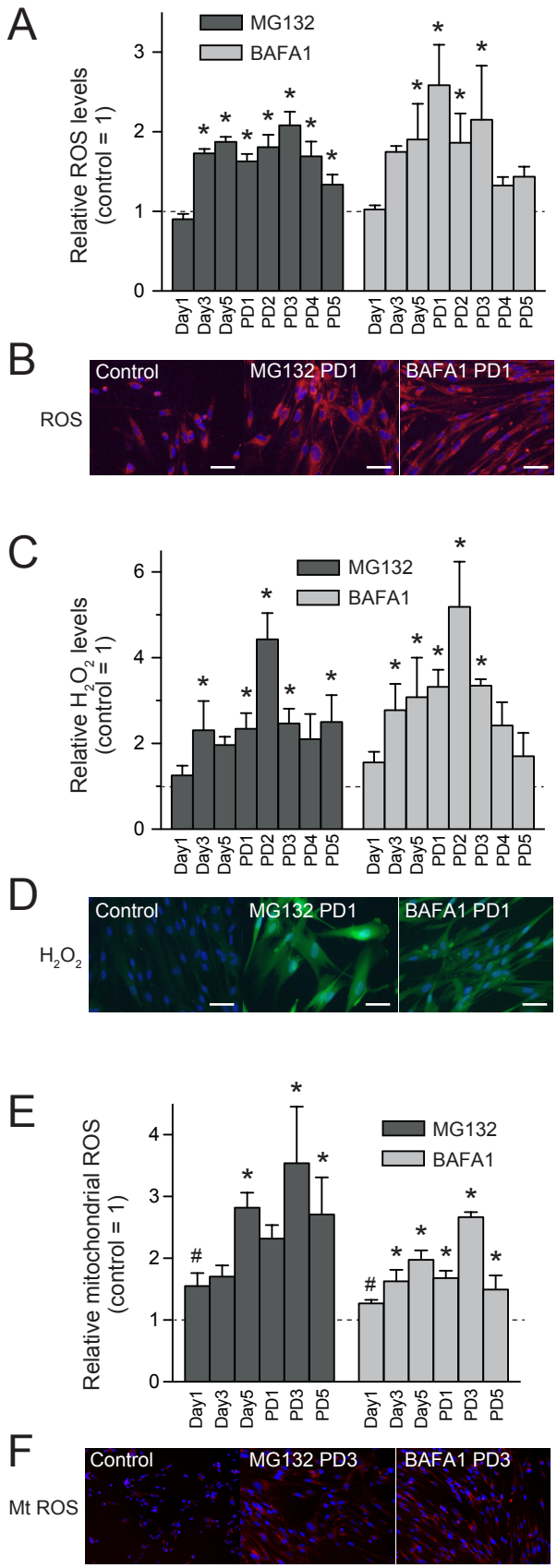
A
MG132
BAFA1
Relative ROS levels
(control = 1)
0
1
2
3
Day1
Day3
Day5
PD1
PD2
PD3
PD4
PD5
B
ROS
Control
MG132 PD1
BAFA1 PD1
C
Relative H_2O_2 levels
(control = 1)
0
2
4
6
D
H_2O_2
Control
MG132 PD1
BAFA1 PD1
E
Relative mitochondrial ROS
(control = 1)
0
1
2
3
4
F
Mt ROS
Control
MG132 PD3
BAFA1 PD3

Figure 3

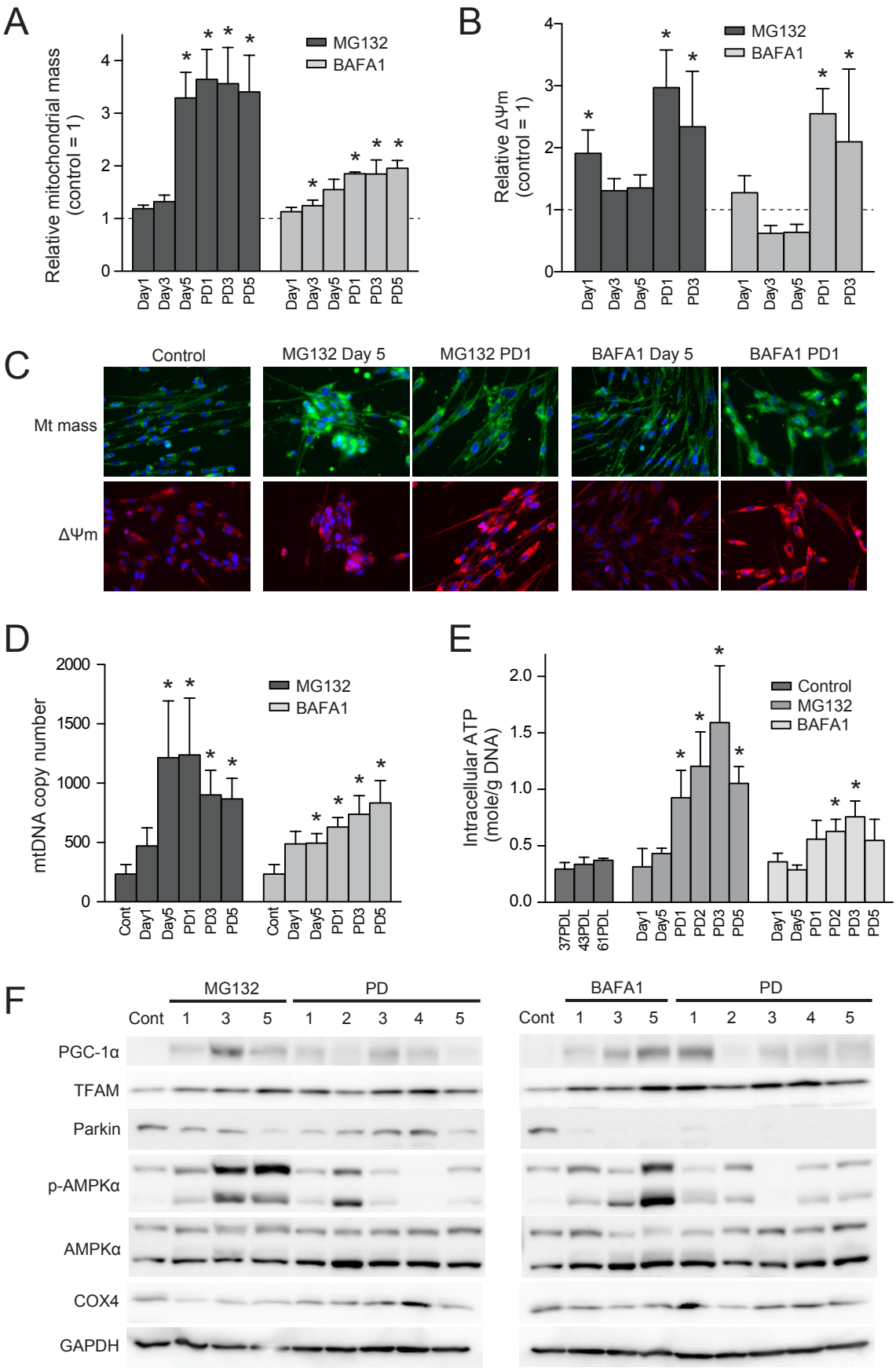
A
Relative mitochondrial mass (control = 1)
MG132
BAFA1
Day1
Day3
Day5
PD1
PD3
PD5
B
Relative ΔΨm (control = 1)
MG132
BAFA1
C
Control
MG132 Day 5
MG132 PD1
BAFA1 Day 5
BAFA1 PD1
Mt mass
ΔΨm
D
mtDNA copy number
MG132
BAFA1
Cont
E
Intracellular ATP (mole/g DNA)
Control
MG132
BAFA1
37PDL
43PDL
61PDL
PD2
F
MG132
PD
BAFA1
PGC-1α
TFAM
Parkin
p-AMPKα
AMPKα
COX4
GAPDH

Figure 4

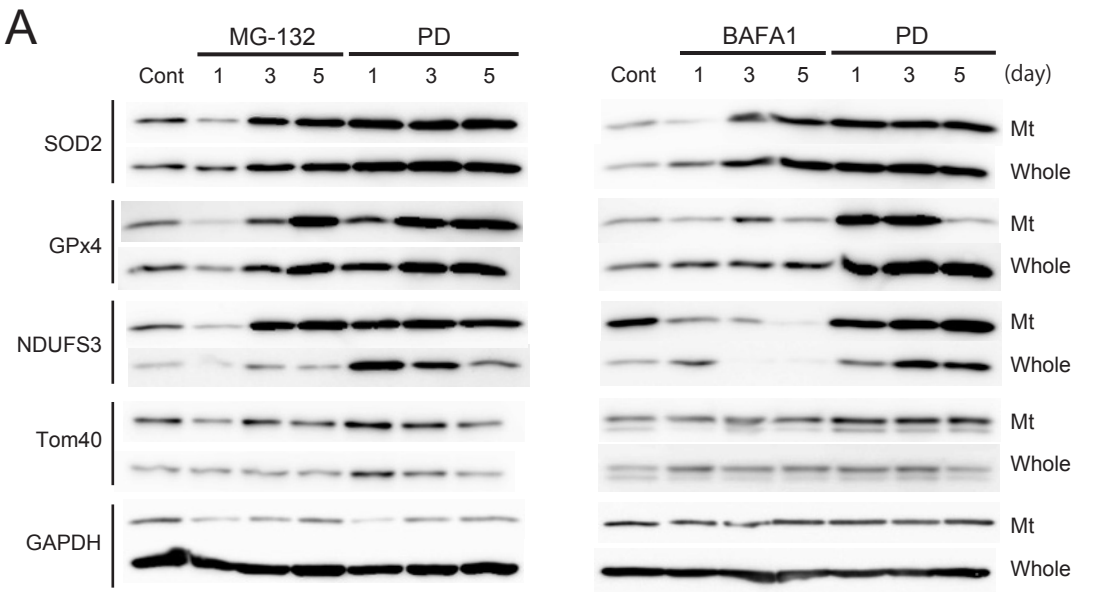
A
MG-132
PD
Cont
1
3
5
1
3
5
BAFA1
PD
Cont
1
3
5
1
3
5
(day)
SOD2
GPx4
NDUFS3
Tom40
GAPDH
Mt
Whole

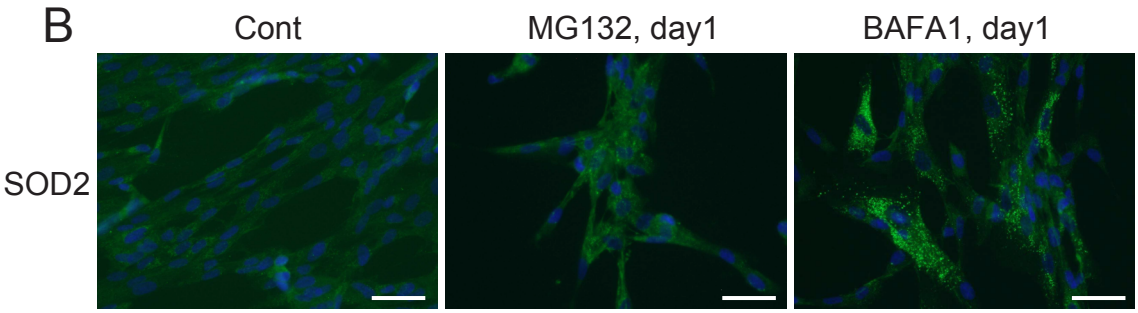
B
Cont
MG132, day1
BAFA1, day1
SOD2

Figure 5

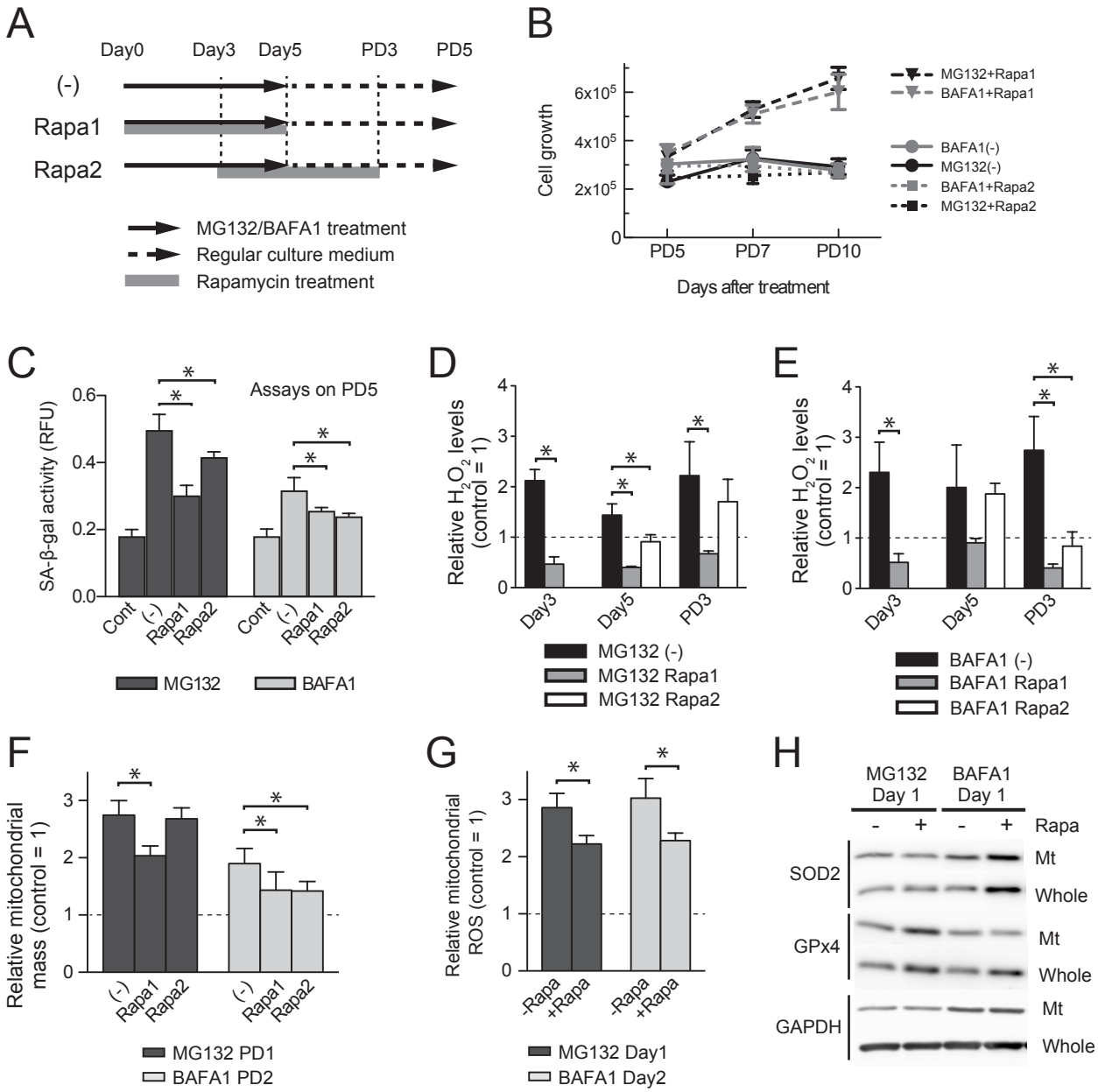
A
Day0
Day3
Day5
PD3
PD5
(-)
Rapa1
Rapa2
MG132/BAFA1 treatment
Regular culture medium
Rapamycin treatment
B
Cell growth
6x10^5
4x10^5
2x10^5
0
PD5
PD7
PD10
Days after treatment
MG132+Rapa1
BAFA1+Rapa1
BAFA1(-)
MG132(-)
BAFA1+Rapa2
MG132+Rapa2
C
Assays on PD5
SA-β-gal activity (RFU)
0.6
0.4
0.2
0.0
Cont
(-)
Rapa1
Rapa2
MG132
BAFA1
D
Relative H2O2 levels (control = 1)
Day3
Day5
PD3
MG132 (-)
MG132 Rapa1
MG132 Rapa2
E
Relative H2O2 levels (control = 1)
Day3
Day5
PD3
BAFA1 (-)
BAFA1 Rapa1
BAFA1 Rapa2
F
Relative mitochondrial mass (control = 1)
(-)
Rapa1
Rapa2
MG132 PD1
BAFA1 PD2
G
Relative mitochondrial ROS (control = 1)
-Rapa
+Rapa
MG132 Day1
BAFA1 Day2
H
MG132 Day 1
BAFA1 Day 1
Rapa
SOD2
GPx4
GAPDH
Mt
Whole

Figure 6

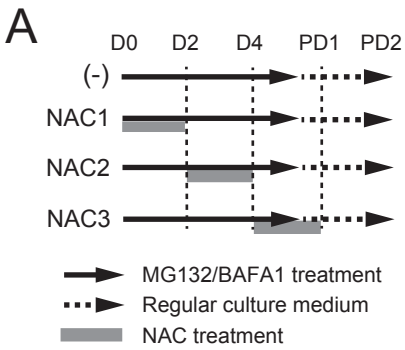
A
D0
D2
D4
PD1
PD2
(-)
NAC1
NAC2
NAC3
MG132/BAFA1 treatment
Regular culture medium
NAC treatment

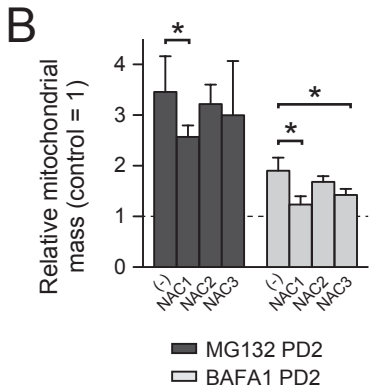
B
Relative mitochondrial mass (control = 1)
0
1
2
3
4
*
*
*
(-)
NAC1
NAC2
NAC3
(-)
NAC1
NAC2
NAC3
MG132 PD2
BAFA1 PD2

Figure 7

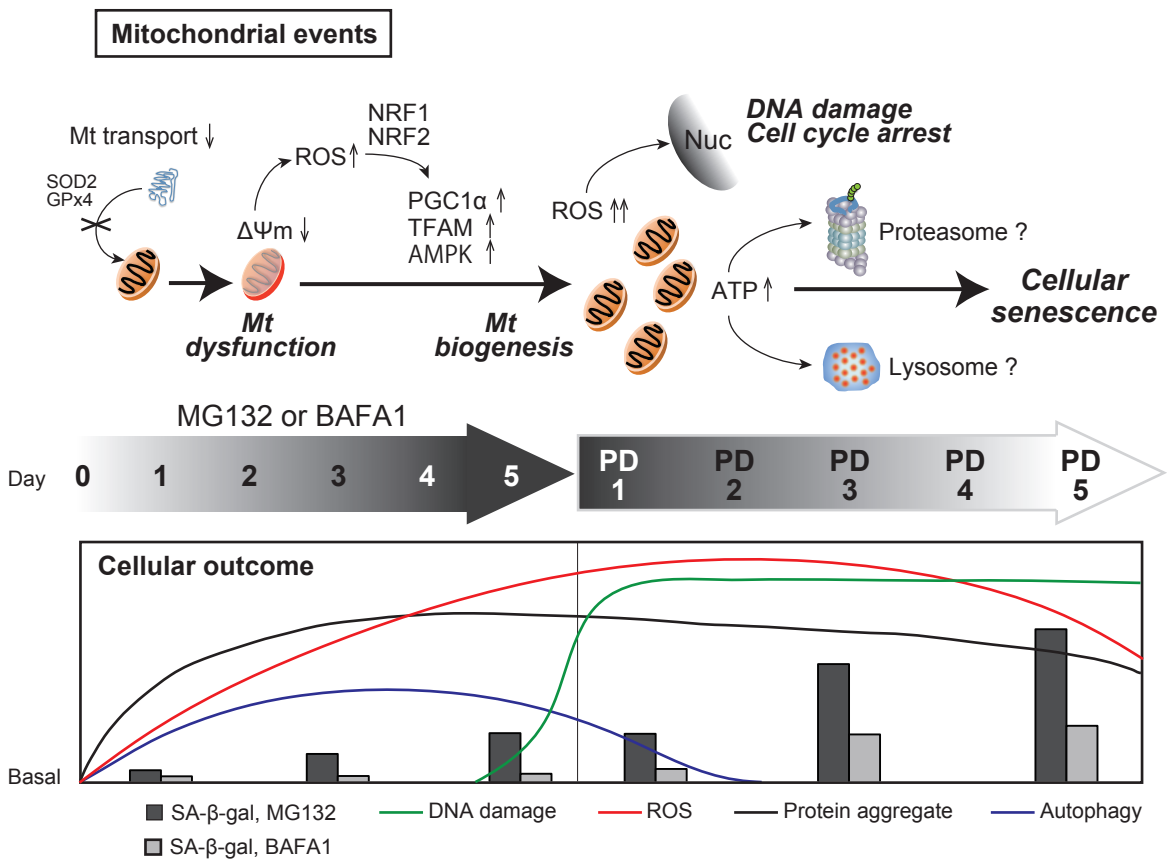
Mitochondrial events
Mt transport ↓
SOD2
GPx4
ΔΨm ↓
ROS ↑
NRF1
NRF2
PGC1α ↑
TFAM ↑
AMPK ↑
Mt dysfunction
Mt biogenesis
ROS ↑↑
Nuc
DNA damage
Cell cycle arrest
ATP ↑
Proteasome ?
Lysosome ?
Cellular senescence
MG132 or BAFA1
Day
0
1
2
3
4
5
PD 1
PD 2
PD 3
PD 4
PD 5
Cellular outcome
Basal
SA-β-gal, MG132
SA-β-gal, BAFA1
DNA damage
ROS
Protein aggregate
Autophagy

Figure S1

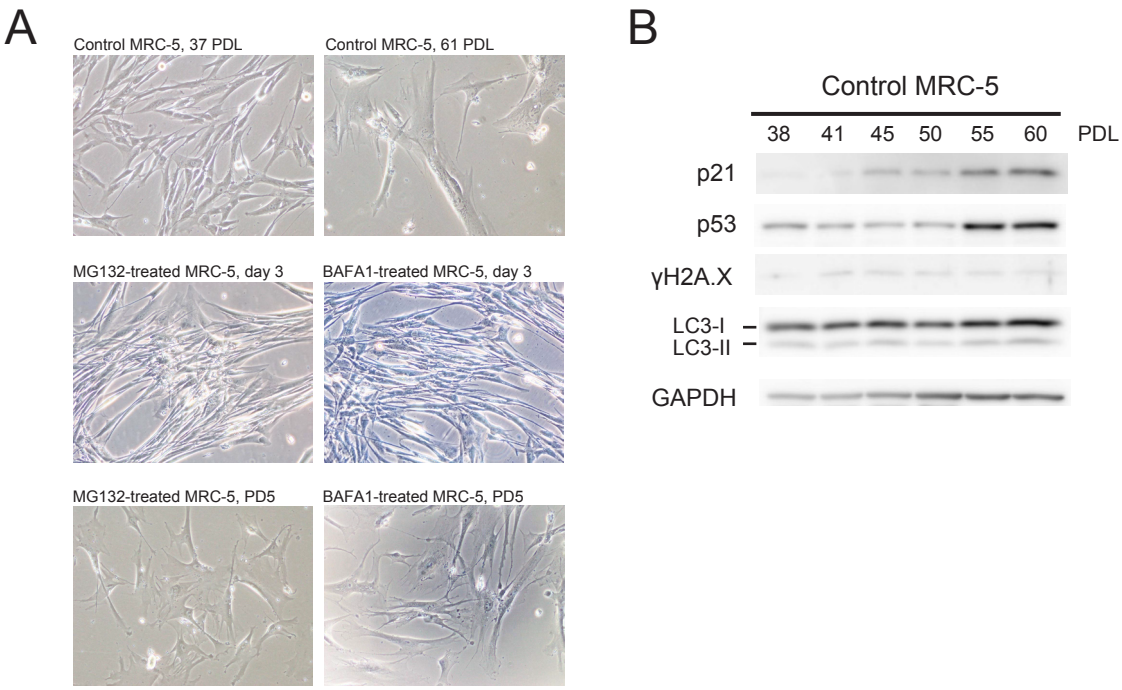

(A) Representative pictures of senescence-induced MRC-5 cells by MG132 or BAFA1 treatment (day 3 and PD5) with young (37 PDL) and aged (61 PDL) control cells.

(B) Immunoblot analysis of untreated control MRC-5 cells undergoing replicative senescence (from 38 to 60 PDL) using antibodies against p21, p53, γH2A.X, LC3,

Figure S2

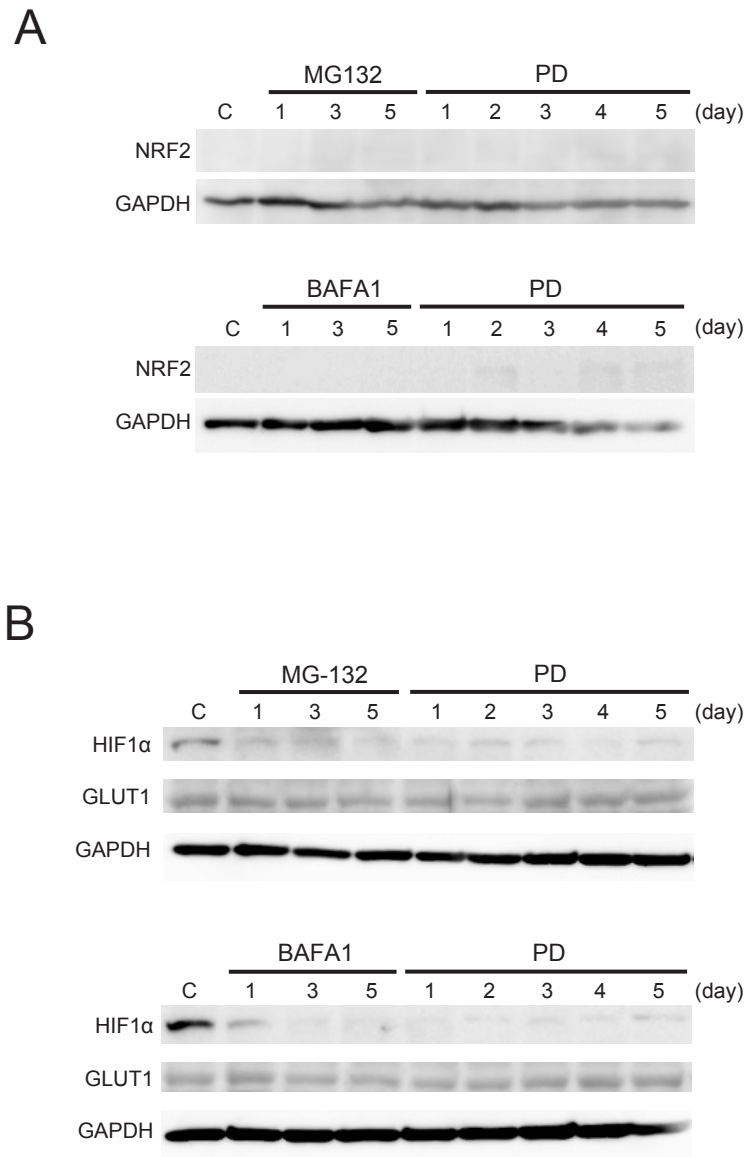

(A) Immunoblot analyses of MG132- or BAFA1-treated cells using antibodies against NRF2 and GAPDH. C, untreated control cells.

(B) Immunoblot analyses of MG132- or BAFA1-treated cells using antibodies against HIF1α, GLUT1, and GAPDH. C, untreated control cells.

Figure S3

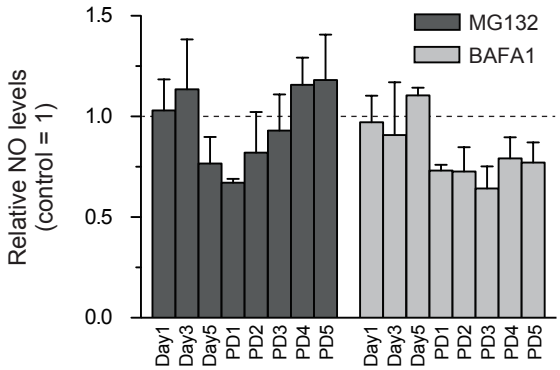

Quantitation of relative intracellular NO levels by using DAF-FM DA fluorescent dye that selectively detects NO. The fluorescence intensity for DAF-FM DA was normalized by total protein concentration. Values are shown as mean ± SD from 4 wells of a 96-well plate.

Figure S4

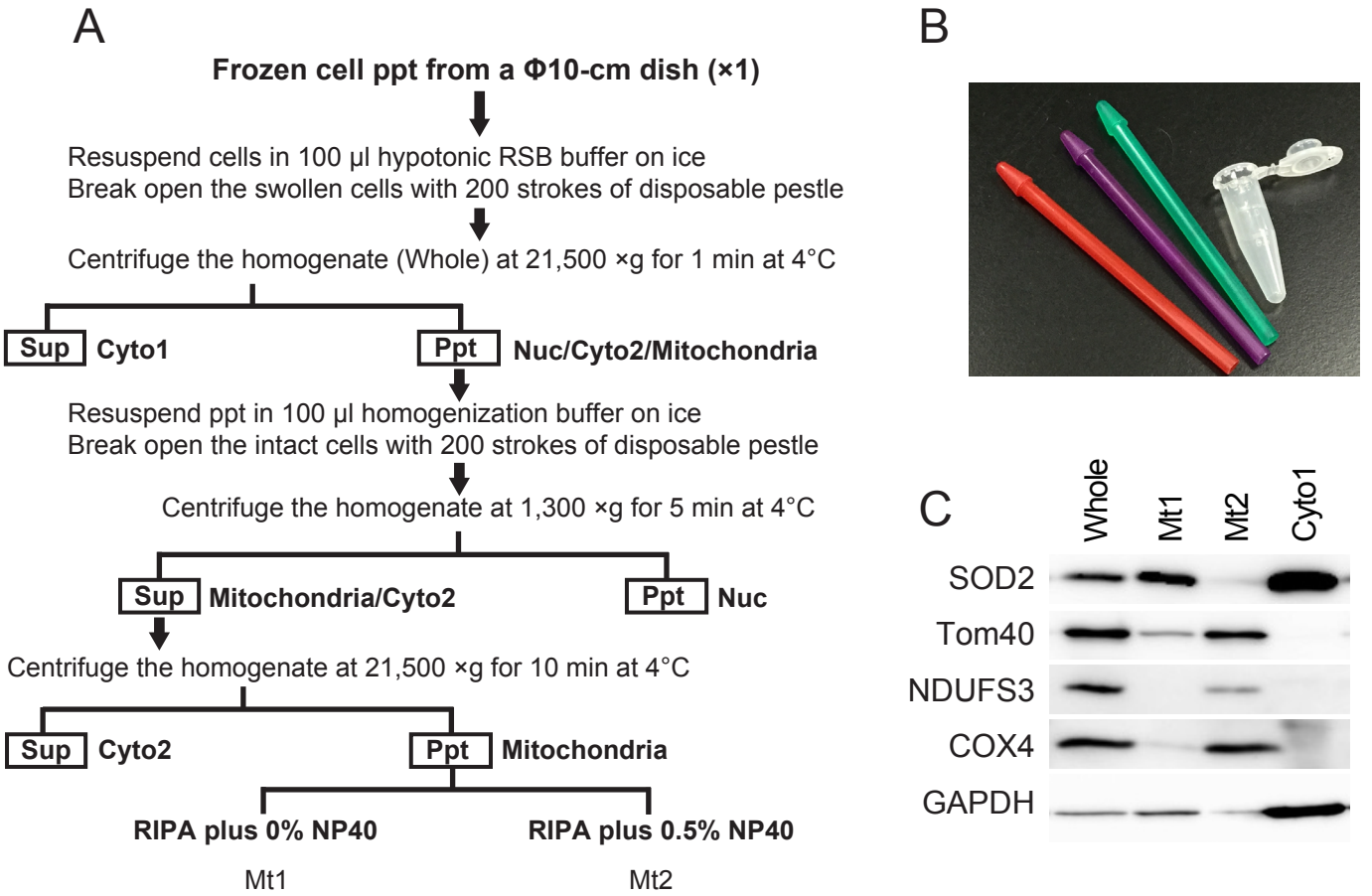

(A) Detailed procedure for preparation of mitochondrial fraction from frozen cell pellet at a microscale. Cells were homogenized in hypotonic RSB buffer, then unbroken cells were repeatedly homogenized in a homogenization buffer. For the immunoblot analyses, solubilized mitochondrial protein in RIPA buffer containing 0.5% NP40 (Mt2) was applied. Hypotonic RSB buffer, 10 mM Tris-HCl, pH7.4, 10 mM NaCl, 1.5 mM $MgCl_2$, protease inhibiter; Homogenization buffer, 5 mM Tris-HCl, pH7.4, 1.5 m$MgCl_2$, 250 mM sucrose, protease inhibitor; RIPA plus 0% NP40, 20 mM Tris-HCl, pH7.4, 50 mM NaCl, 1 mM EDTA, protease inhibitor; RIPA plus 0.5% NP40, 20 mM Tris-HCl, pH7.4, 50 mM NaCl, 0.5% Nonidet P-40, 0.05% SDS, 1 mM EDTA, protease inhibitor; Cyto, cytoplasmic fraction; Nuc, nuclear fraction; Whole, whole cellular extract. (B) Disposable plastic pestles and a matched Safe-Lock tube used in this method. (C) Immunoblot analyses of whole cellular extract (Whole), mitochondrial fractions 1 and 2 (Mt1 and 2), and cytoplasmic fraction (Cyto1) prepared from untreated control MRC5 cells using antibodies against SOD2, Tom40, NDUFS3, COX4, and GAPDH.

Figure S5

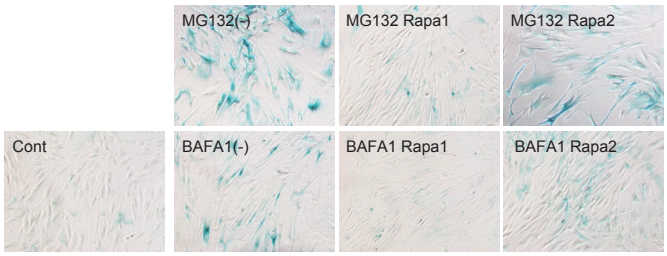

Representative pictures of SA-β-gal positive MRC-5 cells. Cells were co-treated with rapamycin and either MG132 or BAFA1 for 5 days, respectively, and stained at PD5 (cytoplasmic blue precipitate). Control, untreated young (39 PDL) MRC-5 cells. (-), cells treated with only MG132 or BAFA1; Rapa1 and Rapa2, cells co-treated with rapamycin and either MG132 or BAFA1 as shown in Fig. 5A.

Figure S6

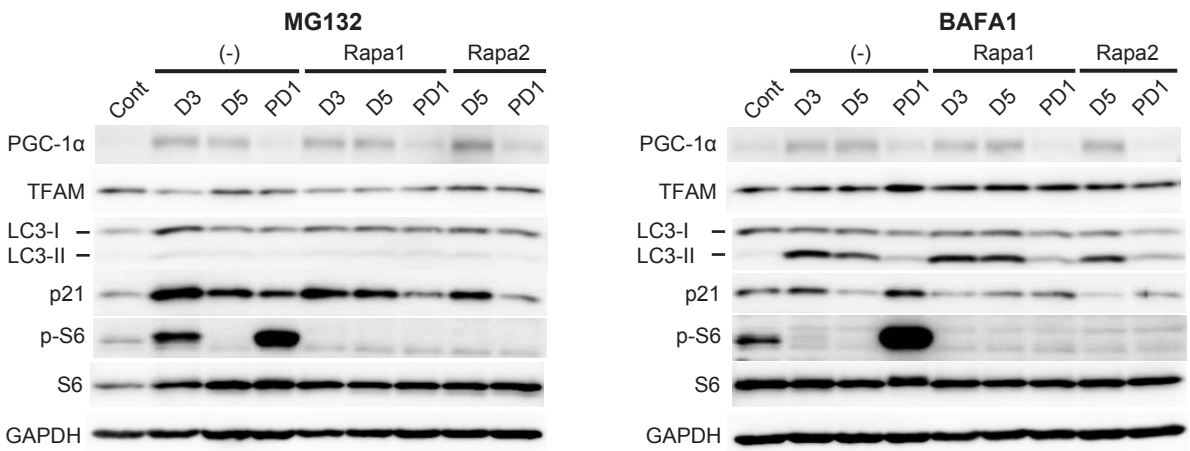

Immunoblot analyses of MG132 (left)- or BAFA1 (right)-treated cells with (Rapa1 and Rapa2) or without (-) rapamycin at day 3 (D3), day 5 (D5), and PD1.